THESIS

A DISTRIBUTED NETWORK OF AUTONOMOUS ENVIRONMENTAL MONITORING SYSTEMS

Submitted by

Kiran Krishnamurthy Kinhal

Department of Electrical and Computer Engineering

In partial fulfillment of the requirements

For the Degree of Master of Science

Colorado State University

Fort Collins, Colorado

Fall 2018

Master's Committee:

Advisor: Mahmood R. Azimi-Sadjadi

Jesse Wilson
Sudipto Ghosh

ABSTRACT

A DISTRIBUTED NETWORK OF AUTONOMOUS ENVIRONMENTAL MONITORING SYSTEMS

Acoustic wireless sensor networks have found applications in various areas including monitoring, assisted living, home automation, security and situational awareness. The process of acoustic detection and classification usually demands significant human involvement in the form of visual and audio examination of the collected data. The accuracy of the detection and classification outcome through this process is often limited by inevitable human errors. In order to overcome this limitation and to automate this process, we present a new fully decentralized decision-making platform referred to as Environmental Monitoring Station (EMS) for sensor-level detection and classification of acoustic airborne sources in national parks. The EMS automatically reports this information to a park station through two wireless communication systems. More specifically, in this thesis, we focus on the implementation of the communication systems on the EMS, and also on the design of $1/3rd$ octave filter bank that is used for onboard spectral sub-band feature generation.

A $1/3rd$ octave filter bank was implemented on the ARTIX-7 FPGA as a custom hardware unit and was interfaced with the detection and classification algorithm on the MicroBlaze softcore processor. The detection results are stored in an SD card and the source counts are tracked in the MicroBlaze firmware. The EMS board is equipped with two expansion slots for incorporating the XBee as well as GSM communication systems. The XBee modules help to build a self-forming mesh network of EMS nodes and makes it easy to add or remove nodes into the network. The GSM module is used as a gateway to send data to the web server. The EMS system is capable of performing detection, classification, and reporting of the source events in near real-time. A field test was recently conducted in the Lake Mead

National Recreation Area by deploying a previously trained system as a slave node and a gateway as a master node to demonstrate and evaluate the detection and classification and the networking abilities of the developed system. It was found that the trained EMS system was able to adequately detect and classify the sources of interest and communicate the results through a gateway to the park station successfully.

At the time of writing this document, only two fully functional EMS boards were built. Thus, it was not possible to physically build a mesh network of several EMS systems. Thus, future research should focus on accomplishing this task. During the field test, it was not possible to achieve a high transmission range for XBee, due to RF interference present in the deployment area. An effort needs to be made to achieve a higher transmission range for XBees by using high gain antenna and keeping the antenna in line-of-sight as much as possible.

Due to inadequate training data, the EMS system frequently misclassified the sources and mis-detected interference as sources. Thus, it is necessary to train the detection and classification algorithm by using a larger and more representative data set with considerable variability to make it more robust and less prone to variability in deployment location.

ACKNOWLEDGEMENTS

First and foremost, I would like to thank my advisor, Dr. Mahmood R. Azimi-Sadjadi, who has looked over many versions of this document patiently and have constantly provided me invaluable feedback and suggestions that have helped in shaping this thesis. He has taught me a lot about signal processing, research and the nuances of technical writing which I believe are important life skills that will help me throughout my career.

I would also like to thank my committee members, Drs. Jesse Wilson and Sudipto Ghosh, for their time and assistance during the course of my research.

I would like to thank the National Park Service (NPS) for supporting my research under the cooperative agreement P14AC01166. I would like to especially thank Dr. Kurt Fristrup for his invaluable guidance that helped in shaping the direction of this Project.

I would like to extend my special thanks to Jarrod Zacher, who has guided me throughout the course of my thesis and particularly for his contributions in finalizing the hardware and the EMS website. Without his constant guidance and support, it would not have been possible to accomplish this work.

I would like to thank Jack Hall for proofreading some of the chapters of this document and also for his constant brainstorming sessions in the lab, which has helped to enhance my learning experience at CSU. I would also like to thank Aanand Thiyagarajan for proofreading Chapter 4 of this document.

I would also like to thank Ashley Pipkin for helping me with the field test during my visit to the Lake Mead National Recreational Area in June 2018. I would also like to thank my dear friend, Shashank Satyanarayana for driving me to the site and for helping me conduct the field test.

Finally, I would like to sincerely thank my parents and my sister for their unwavering support and guidance throughout my entire education.

DEDICATION

I would like to dedicate this thesis to my parents, Krishnamurthy, Vijalayakshmi and my sister Kruthi.

TABLE OF CONTENTS

LIST OF TABLES

LIST OF FIGURES

CHAPTER 1

INTRODUCTION

1.1 Problem Statement and Motivations

Acoustic wireless sensor networks have found applications in various areas including noise monitoring [1], [2], surveillance [3], [4], home automation [5] and also in assisted living [6]. The problem of acoustic detection and classification is often complicated by various factors including, a presence of a large variety of sources, environmental influence on the acoustic signatures of these sources and a lack of availability of adequate data to train the algorithms that perform these operations. The networking ability of these sensors is limited by the communication range of the wireless modem that is employed, which is often affected by the RF interference in the surrounding area and also by other environmental factors such as weather and terrain shielding.

The work in this thesis focuses on an acoustic wireless sensor network that performs autonomous aircraft identification and reporting. The motivation for this work is drawn from a cooperative agreement with the National Park Service (NPS), which is currently interested in monitoring noise pollution in national parks, caused mainly by man-made airborne sources and to study its effects on the park ecosystem. More specifically, the goal of this work is on the development of an Environmental Monitoring System (EMS) which is designed to identify and count the number of airborne sources and report these events wirelessly to a park station.

Currently, the NPS performs this analysis by using expensive and bulky sound meters designed by Larson Davis [7]. The process involves, deploying these devices along with audio recorders in remote places to capture $1/3rd$ octave spectral data and audio timeseries pertaining to the sources of interest. The collected data is then post-processed manually by

experts by visual examination of the $1/3rd$ octave spectral data or listening to the time-series to locate and label the sources. This process usually involves manual sorting of hundreds of hours of acoustic data which is extremely laborious. Moreover, to obtain an accurate noise map of the national park, it is essential that the data is collected and sources are labeled in various parts of the national park. Hence, the approach employed by the NPS to perform source detection and classification is not scalable.

In this work, we plan to overcome these limitations by using an ARTIX-7 Field Programmable Gate Array (FPGA) based EMS system [8] which not only can perform in-situ detection and classification of the sources of interest but also can report these events automatically to the park station via onboard wireless communication systems. The main focus of this thesis is on the development of the hardware, software and the firmware around the communication systems of the EMS system, in order to enable forming a network of several EMS nodes that can be deployed, unattended for an extended period of time. The detection and classification on the EMS system is performed in near real-time and the results are stored in an SD card and reported to the park station once every few hours. Each EMS node comes with a GPS module which provides accurate coordinates of the sources and the system is also equipped with a Real Time Clock (RTC) which helps in time-stamping the occurrences of these sources.

The EMS system is designed to be solar powered during the day and battery powered at night. The EMS systems are designed to operate on a range of voltages from $3.3V$ to up to $15V$, which makes it possible to use a wide range of batteries. The EMS system is also equipped with a charge controller circuitry, which can be used to charge the battery from solar panels during the day. This ensures that EMS systems can perform acoustic monitoring for long periods of time without requiring a lot of human intervention.

This thesis mainly focuses on the development of firmware and software for the communication modules and their integration with the detection and classification algorithm that is implemented on the EMS system. Each EMS system is equipped with two expansion slots

to accommodate XBee and GSM modules. Only the gateways (master) are equipped with the UBLOX SARA-U260 GSM modules to reduce overall cost, while all the nodes (slave and master) are equipped with XBee modules. The XBee module (Digi International XBee PRO S3B) is mainly adopted by the slave nodes to communicate with other nodes in the network as well as with the gateway. The master node then accumulates these reports and transmits them to a web server, where the results are displayed and stored. This enables the EMS systems to be deployed in remote areas with poor cellular connectivity, so long as the slave nodes are able to route data to the master node using XBee transceivers.

1.2 Literature Review on Acoustic Wireless Sensor Networks

A bulk of the material in this section is referred from [8].Several systems have recently been developed and prototyped to provide different acoustic/sonar detection, classification, and/or tracking capabilities. The system in [9] was developed to track dolphin population and habitats using an array of hydrophones attached to the rear of a boat. The FPGA core in this system is mainly used for data acquisition and buffering while the bulk of the processing including wavelet-based filtering, detection, and bearing angle estimation are implemented on a laptop. A perceptron neural network computes the range and bearing angle associated with the detected underwater source. The system is not decentralized and lacks networking capabilities, power management, and source identification capabilities. In [10], the authors of [9] designed a virtual system using 3 hydrophone array for tracking and localizing the dolphin's vocalizations. In this system, the localization is achieved with the help of two GPS modules and the authors used PocketPC iPAQ hp2700 to acquire and digitize the acoustic data from the hydrophones. The communication was achieved by first projecting the sound to the base ship and the data is then sent to a web server using a Wi-Fi network that includes both the remote device and a base station and an additional access point with a high-gain antenna in order to extend the Wi-Fi network range. The

range of the WiFi-based communication employed in this system is not nearly as high as the GSM module used in our EMS system. Furthermore, it requires that base station and the remote system to be fairly close to each other. The system uses wavelets and neural networks for analyzing the audio data and all the post-processing is done in the base station using a laptop. This system lacks real-time source tracking and localization capabilities and does not possess any networking features. In [11], the authors proposed a three-tier decentralized low-power wireless sensor network solution for vehicle classification using their acoustic signatures. The first tier consists of clusters of wireless sensor nodes (e.g., Mica2 motes) sending the collected data to gateway cluster heads which in turn perform feature extraction and preliminary decision-making. The third tier is the base station integrated with other base stations via the Internet to perform high-level decision-making, decision fusion, and network management. The main goal of the design is to reduce the power consumption of wireless sensor networks to distribute the processing among cluster-heads and the base stations. The system employs power-detector, spectral features, and Support Vector Machine (SVM) [12] for event classification. Although the system offers acoustic event classification similar to the EMS, it is structurally and algorithmically different, in many ways. It relies on deploying a multitude of clusters of wireless sensor nodes, gateways, and base stations communicating through wireless local area network (WLAN) and Internet access. The nodes dont use FPGA boards and lack many capabilities of the EMS system including microphone array processing and source trajectory estimation. In [13], the authors proposed a system for of wireless sensor network for detection of bird species, logrunners in particular. The detection algorithm is based on a likelihood ratio test between statistical models of the target and non-target audio frames, similar to the EMS. The feature extraction is done in this system by passing the signal through Hamming window and then compute short time power spectrum of the windowed signals as opposed to EMS where we use $1/3rd$ octave filtering and calculate Sound Pressure Level (SPL) for each of the 33 sub-bands. The authors have only mentioned that the algorithm has been implemented on CSIROpsilas

wireless sensor network platform, which does not describe the communication scheme clearly. The authors in [6] proposed an Ambient Assisted Living (AAL) system, where they perform onboard acoustic detection and classification of the urban noise map related to vehicle traffic, indoor gunshots, etc, on the ESP32 platform. The authors employ the WiFi chip available on the ESP32 board to achieve networking among the sensor nodes. Because of the low communication range of WiFi, it is required that the sensor nodes always remain close to the base station, which indeed is a limitation. Moreover, the system is only able to process acoustic data up to $5kHz$ as the maximum sampling rate that was achieved was only $10kHz$. The EMS system, on the other hand, has a $1/3rd$ octave filter bank built on the ARTIX-7 FPGA, which is able to achieve sampling rates up to $100kHz$ and thus, enabling it to process the entire audio spectrum effortlessly. Sallai et. al [14], designed an FPGA-based helmet-mounted sensor node for counter-sniper applications. The sensor board supports four microphone channels forming a small array for computing the angle of arrival (AoA) of the muzzle blast and ballistic shockwave wavefronts using the time of arrival (ToA) estimates for each microphone. The fusion algorithm at a base station then estimates the shooter location, bullet trajectory, and caliber, as well as the weapon type using the received information from multiple nodes forming an ad-hoc network. Although there are some similarities between their sensor node and the EMS architectures, their functionality and applications are different. Finally, in [15], [16] the authors developed different neural network-based algorithms for the detection and classification of ground and airborne vehicles without providing any hardware structure for their implementation.

1.3 Technical Contributions of the Present Work

The main contributions of this work include: (a) implementation of $1/3rd$ octave filter bank to generate onboard spectral sub-band features in near real-time, (b) development of communication system firmware and its integration with the detection and classification algorithm and (c) the integration of the onboard sensor suite with the rest of the system

to enable the EMS to detect, classify and send aircraft and environmental data to a park station autonomously. The EMS is an ARTIX-7 FPGA based system that is equipped with inbuilt GPS and Real Time Clock (RTC) modules, which can be used to localize the source events spatially and temporally. The onboard sensor suite enables monitoring of various environmental parameters such as pressure, temperature, ambient light, etc.

The $1/3rd$ octave filter bank was implemented in the FPGA as a custom hardware unit and the code was written in VHDL. The filter bank is designed to be compliant with the ANSI S.11 standards and is IEC class 0 accurate. The filter bank samples the acoustic signals at $50kHz$ and decomposes the entire audio spectrum into 33 sub-bands and Sound Pressure Level (SPL) for each sub-band is computed and converted to dB . The Sparse Coefficient State Tracking (SCST) [17] algorithm which is implemented on the MicroBlaze softcore processor uses the energy values computed for these spectral sub-bands to perform detection and classification. The $1/3rd$ octave data along with the classification results (source labels) are stored in the SD card which is interfaced with the FPGA through Serial Peripheral Interface (SPI) protocol. Additionally, an analysis of the effects of quantization error present in the $1/3rd$ octave filter bank was made and the strategies that can be employed to minimize these errors were discussed.

The EMS system is designed and built to function as a fully decentralized acoustic sensor network. Each EMS node is designed to have two expansion slots to accommodate the XBee and Global System for Mobile (GSM) communication modules. The XBee in the EMS system makes it possible to build a self-forming mesh network, where new EMS nodes can be added or existing nodes can be removed without disturbing the functionality of the overall network. The GSM module makes it possible to route the classification results to any part of the world, so long as there is cellular connectivity in the deployment area. Every EMS node in the network is capable of autonomously performing detection, classification, and reporting of the aircraft events, hence performing collaborative decision making. Only the nodes that are equipped with the GSM module can function as a gateway to the park station, while

the other nodes in the network route the classification reports to the gateway. The GSM module transmits data in General Packet Radio Service (GPRS) mode to minimize power consumption and cost.

The EMS system is only required to send the classification reports once every few hours. Thus, the communication systems are programmed to operate in idle mode during most of the system's operating period. The idle mode operating current of both XBee and GSM modules used in this system is very low (in the order of micro-amps) and their contribution to the overall power profile of the system is negligible. This is done to make sure that the EMS system can be deployed for extended periods of time, even while battery powered, by avoiding unnecessary power consumption.

An interrupt control logic was developed to successfully integrate the entire system. The developed logic takes care of all the failure cases and makes sure that the interrupt sources present in the EMS systems are controlled in such a way that they do not affect each other and do not cause the system to malfunction. This logic can be further extended when new subsystems or features are added to the EMS system.

A simulation of XBee mesh network was performed by collecting realistic data to accurately estimate the communication range of XBee transceivers and also to analyze the effect of location of a node failure on the packet loss percentage. The simulation was performed by configuring the parameters in such a way that the effects of RF signal reflections due to the ground and other interference sources were accounted for, while estimating the transmission range of the XBee modules.

Two fully integrated EMS systems were tested at Indian Pass in Lake Mead National Recreation Area in Arizona. The system had been previously sent (in July 2016) to a different site in the same park and deployed there for nearly 48 hours to collect $1/3rd$ octave data. The data related to the sources of interest was then manually annotated by visually examining the $1/3rd$ octave spectrum and by listening to the audio series. The EMS system was trained by using this labeled data. The training involved building the dictionary matrices using the

K-SVD algorithm [18] for different source and interference types present in that particular site. The log-likelihood ratio values were computed for each Bayesian network [19] source model. The dictionaries and the log-likelihood ratios were then stored in the flash memory of the EMS system. The trained system was then recently (June 2018) deployed in a different location for nearly 25 hours in Lake Mead National Recreation Area. In this field test, a full system test of the EMS sensor network was performed where the EMS system performed autonomous detection and classification of the sources of interest and sent these reports to a web server by using onboard wireless modems. The reported data was automatically plotted on the EMS website (`emsys.colostate.edu`) to enable the NPS to continuously monitor the air traffic and the surrounding environment. The system was also able to simultaneously record the classification results and the $1/3rd$ octave spectral data onto on SD card.

1.4 Thesis Organization

This thesis is organized as follows: In Chapter 2 a full system overview of the EMS system is presented. This chapter addresses the hardware capabilities and the core software design principles that were employed in writing the firmware for the EMS system. Chapter 3 provides a brief overview of the design of FPGA based $1/3rd$ octave filter bank [20]. This chapter also focuses on addressing the effects of quantization error on the filter bank and discusses an alternative filter design methodology that can help in overcoming the quantization errors. Chapter 4 focuses on the design and analysis of the communication systems used in the EMS system. Chapter 5 presents the results and analysis of the field test that was conducted in Lake Mead National Recreation Area. Finally, in Chapter 6, a summary of findings discussed in this thesis and an outline for potential future work is presented.

CHAPTER 2

EMS FULL SYSTEM OVERVIEW

2.1 Introduction

The current method employed by the NPS to record the aircraft events involves deploying a sound meter designed by Larson Davis in the field for a few days and then manually retrieving the equipment. The retrieved $1/3rd$ octave data is then post-processed to identify sources. Larson Davis [7] sound meters and the microphone attachments that come with these sound meters are expensive and bulky. Additionally, they don't have any processing and communication capabilities to automatically identify the source events during deployment. Thus, there is a huge time gap between the time events are recorded versus the time events are finally identified and reported.

The main purpose of the EMS system is to eliminate these shortcomings. Additionally, the EMS is designed to operate in such a way that it requires no human intervention whatsoever except in case the system is broken by an animal or if there is a complete power loss. The Xilinx Artix-7 FPGA which sits on the EMS system computes the $1/3rd$ octave data using a filter bank built into it. The recorded $1/3rd$ octave spectral data is further processed using onboard event detector and classifier [21]. The results are then reported to the park station in near real-time. In addition, the EMS system has the ability to beamform data from multiple microphones forming an array to track the classified sources to generate their approximate flight paths. This feature is enabled by having five stereo channels supporting ten microphones in total. Both azimuth and elevation angles can be generated using the beamforming algorithm [8]. This automated reporting would eliminate the need for manual collection of data and would allow NPS to make quicker and more frequent soundscape updates. The cost of EMS in comparison to Larson Davis is substantially lower while the form

factor is much smaller. These features enable NPS to deploy a large number of these devices at different park sites, forming an intelligent network to detect and classify aircraft events and generate a much better event map compared to the Larson Davis approach.

This chapter will give a brief overview of how the EMS system is designed and operated. Section 2.2 focuses on describing the EMS hardware and its capabilities. Section 2.3 focuses on the core of the software design principles employed in writing the firmware for EMS. Concluding remarks are given in section 2.4.

2.2 Hardware Description and Capabilities

The EMS system is a novel acoustical monitoring system which continuously monitors aircraft activity by analyzing acoustical data [8]. It comprises multiple channels through which the data can be fed into it and also enables tracking of the direction of detected sources [22]. The EMS system has an onboard sensor suite which lets the park service know of various parameters related the surrounding environment such as temperature, pressure, light, acceleration, wind speed/direction, digital compass and it also has a GPS module embedded into it. The module also comes with an embedded real-time clock (RTC) which enables the time stamping of the events. The heart of the EMS system is the Artix-7 FPGA which performs $1/3rd$ octave filtering and contains all the necessary glue logic. The system is equipped with two communication expansion slots which enable the inclusion of high-performance radio and cellular links. The modalities can then be used to form a mesh network and to send updates to the park station automatically. The system overview of the EMS system is shown in Figure 2.1 [8].

The data acquisition subsystem consists of InvenSense ICS-43432 which outputs 24-bit digital data at 48,000 samples per second. This particular microphone was selected because of its high dynamic range and low cost. The microphone has nearly a flat magnitude response up to $10KHz$ as shown in Figure 2.2 [23]. For this particular application, the maximum frequency that we are concerned about is less than $10KHz$. So, we are able to use this

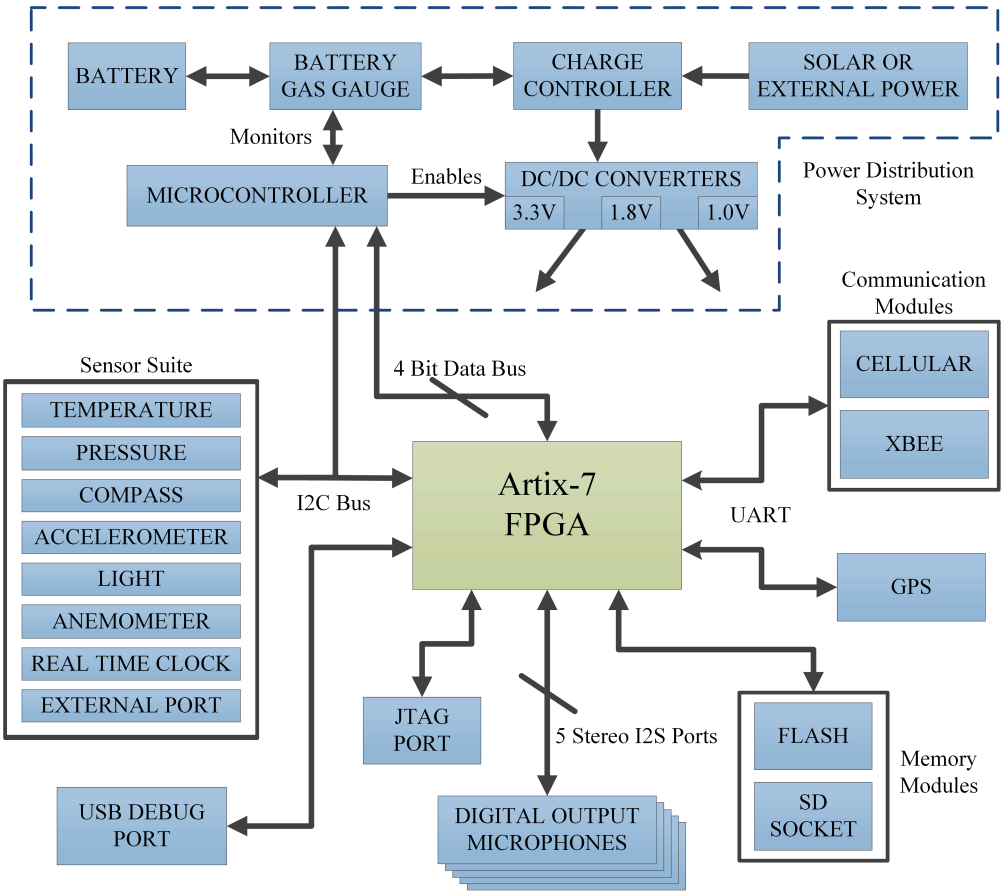

Figure 2.1: EMS System Overview.

microphone without sacrificing any of the functionalities. However, EMS can also be used with other microphones for other possible applications that require higher frequencies greater than $10KHz$, for example, gunshot location finding.

Figures 2.3 and 2.4 show the top and bottom views, respectively with all the components that are present in the EMS system. The main processing powerhouse of the EMS system is the ARTIX-7 FPGA, which allows for easy logic reconfiguration and extensions. The ARTIX-7 FPGA is responsible for both the $1/3rd$ octave filtering as well as the glue logic which binds the entire system together. While the number of logic cells in the FPGA employed in the actual PCB is sufficient, it has only 608KB of inbuilt RAM. Hence an additional nonvolatile flash memory block of 256MB was added to the system. This flash memory stores the bit-stream and also the data file which contains the look-up table. This

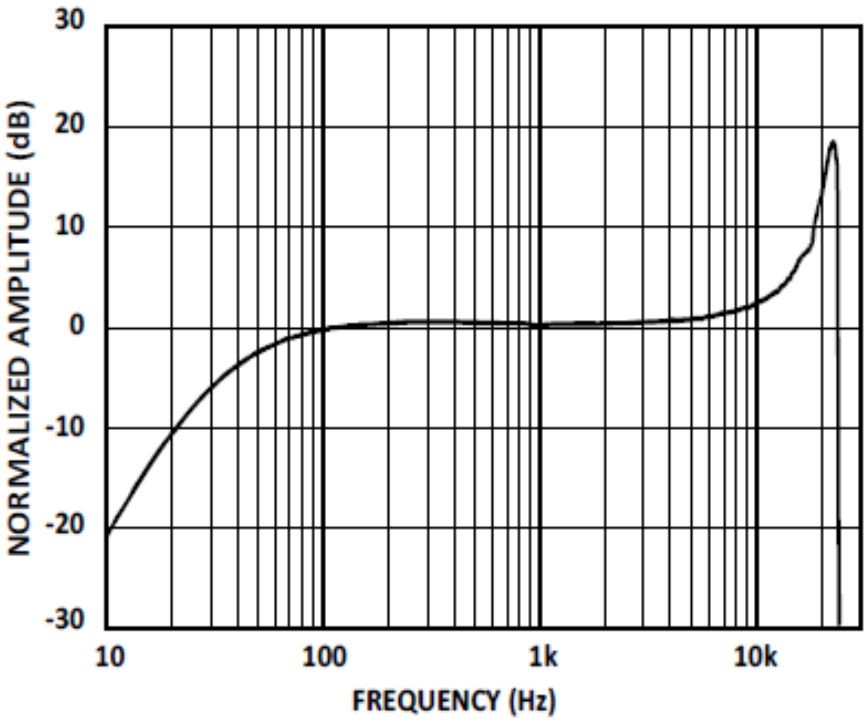

Figure 2.2: InvenSense ICS-43432 Magnitude response.

look-up table contains a static value of the log-likelihood ratio values computed as a part of the SCST algorithm [17] for source detection and classification. The FPGA unit has 300 digital IO ports which enable us to interface it with a number of peripherals including the SD card and the sensor suite. The SD card slot interfaces with the FPGA with the standard SPI protocol, all the processed data including the $1/3rd$ octave data, the noise log-likelihood ratios (NLLR), the signal log-likelihood ratios (SLLR) and the detection results are stored in the SD card as a backup in addition to reporting these events to the park station through a cellular modem. SD card can also be used to store the system configuration parameters which can be specific to different applications.

After the acoustic data is processed in the $1/3rd$ octave block, it outputs data for all the 33 frequency bands. There is a conversion state machine [24] that is implemented in the FPGA which then reads in this data and converts each entry of the matrix from 35 (28 fractional, 7 integer) bit fixed-point to 32-bit floating point representation. Xilinx inbuilt IP cores have been used in this process to make sure we avoid any overflow/underflow errors

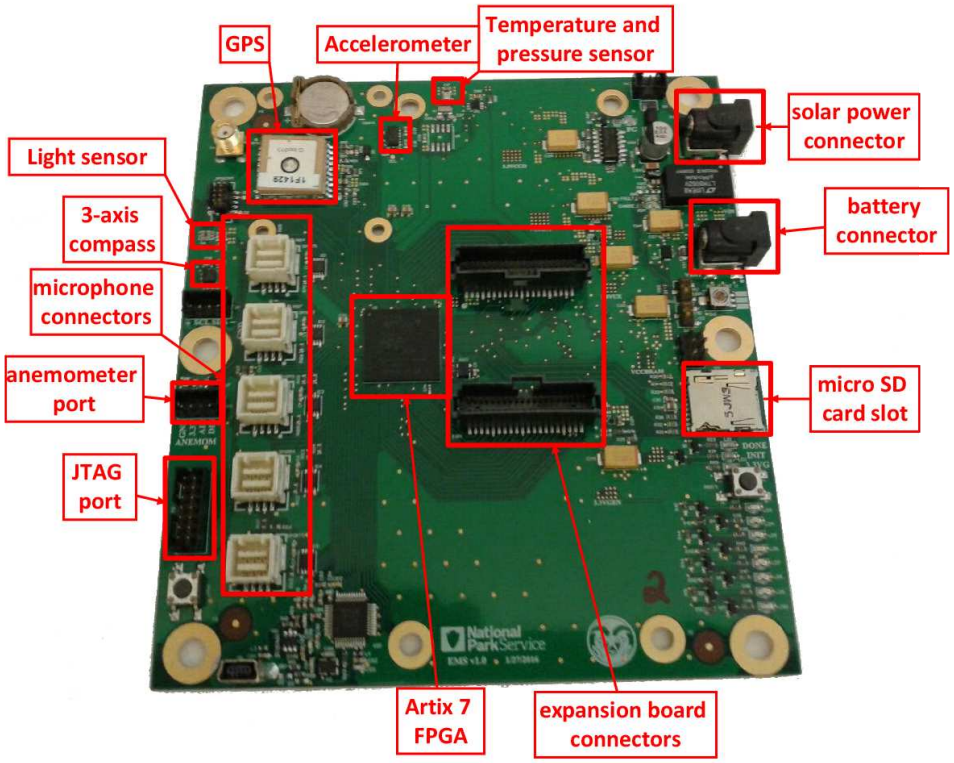

Figure 2.3: Top view of the EMS board.

during this process. This 32-bit floating point data-stream is then used for energy calculation for each sub-band. The sound power level (SPL) in decibels (dB) is given by,

$$L_w = 20log_{10}(P/P_0) \tag{2.1}$$

where P is the total power at a frequency band in root mean squared (RMS) representation and P_0 is the reference sound power also known as the effective input noise (EIN) of the microphone. The value of P_0 is obtained from the data sheet of InvenSense ICS-43432 microphone.

The EMS system is intended to be deployed in the remote locations where it can perform detection and classification entirely on its own. To make sure that this happens smoothly, it is essential that the power system for this system be robust. The EMS system as seen in Figure 2.1 has two power slots. One for battery and the other for solar/wall power. The

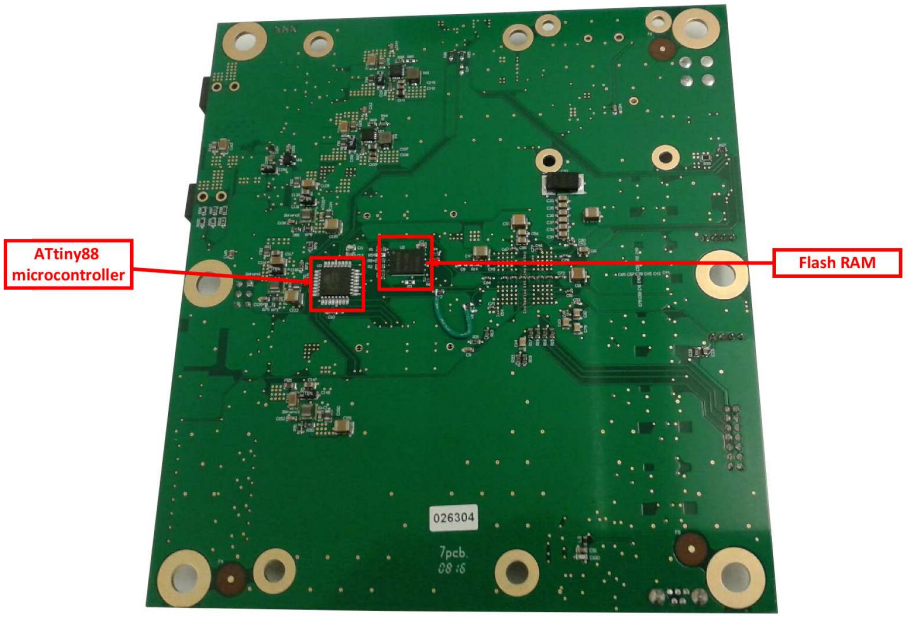

Figure 2.4: Bottom view of the EMS board.

barrel jack DC input accepts voltages ranging from 3.3 V (battery) to 5V (solar/wall power). The light sensor can be used to make decisions as to when to switch from solar to battery mode. There is also a charge controller circuitry built into the system which in case of excess solar power can be used to charge the battery. The solar panel also comes with an MPPT (maximum power point tracking) module which can be used to ensure optimal power profile while using the solar mode. The battery also comes with a gas gauge to constantly monitor the amount of charge in the battery, which can then be used to assess the power consumption. The main idea is that the EMS system should mostly operate on solar power during the day and switch to battery at night. The power sequencing and the bitstream programming of the FPGA board are controlled by using Atmel ATtiny88 microcontroller.

2.2.1 Communication Sub-System Overview

Another important highlight of the EMS system is its ability to detect and classify data, prepare reports and automatically send them to a cloud hosting platform. In addition to

this feature, when a number of EMS systems are deployed in the field, they are able to form a mesh network and function as a decentralized network of intelligent agents. Each EMS system comes with two expansion slots, one for XBee and the other one for the GSM module. It is important to note that not all the EMS are required to have GSM modules, except the modules that communicate with the base station.

The Zigbee radio module that is currently being used is XBee PRO S3B by Digi International, which is used for WLAN communication of all the information including sensor data, logistics of a number of man-made airborne vehicles and system health. XBee communication is mainly used by slave modules to communicate with the anchor (Master) module in a particular distribution network. In a network of sensors, such as the EMS system, it is necessary for the Master module to be able to communicate with various slave devices to accumulate and transmit data to the base station. Hence, the XBees of the Master and Slave devices are configured in the Application Programming Interface (API) mode . In this mode, data is communicated in a structured manner in the form of organized packets and in a determined order which will be clarified in Section 4.2. This functionality allows us to not have to define our own protocol in a complex communication network such as EMS sensor network. API mode also allows the modules that receive information wirelessly to identify the source, which is necessary to pinpoint the actual location of the source event that has occurred, as all the modules are equipped with GPS functionality. In API mode we can also find out the signal strength of each received packet to dynamically estimate the link strength. Moreover, API mode enables us to gather information related to packet loss and we could also send firmware updates from a remote location or configure other XBees in a particular local network, if necessary.

Upon reception of packets sent by slave modules, the master module now has to update these values in the online server. The Master module has both XBee and GSM functionality. The GSM module on the EMS is the UBLOX-SARAU260, which is first configured in General Packet Radio Service (GPRS) mode. The HTTP requests are then sent to the server to

enable the server to receive the packets sent by EMS system. GPRS supports TCP/IP mode of operation. We send the data in this mode which automatically takes care of the pauses during handover and packet losses are handled by the TCP protocol. In particular, the system uses HTTP POST messages at the application layer to transfer data between the base station and web server. Using the POST method, the EMS system creates and sends requests to a web server to store reports contained in the body of the POST message. The server stores all report data in a structured query language (SQL) database. Queries can then be made against the database for further data analysis and visualization. The EMS system coupled with XBee and GSM modules is shown in Figure 2.5.

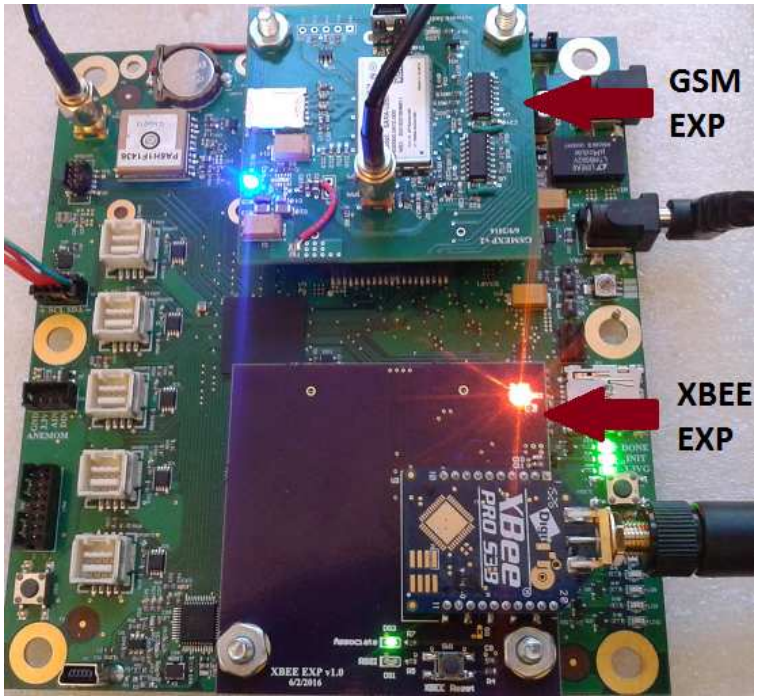

Figure 2.5: EMS System with XBee and GSM expansion modules.

2.2.2 Sensor Suite Overview

In addition to performing acoustic monitoring, EMS is also capable of collecting general environmental data by the use of an onboard analog sensor suite shown in the Figure 2.1. All the sensors are interfaced with the ARTIX-7 through an IIC interface. In the version 1.2 of the EMS, however, the IIC line enable pin is controlled by the microcontroller Atmel

ATtiny88. EMS has an inbuilt barometric pressure sensor (bmp280) which monitors the air pressure. There is also an inbuilt temperature sensor which is used to monitor the PCB temperature. There is a provision to mount an external temperature sensor (LM75B) to monitor the environmental temperature. The system is also equipped with the HMC5883L 3-axis compass which provides a precise orientation of the system. This information is valuable to the beamforming algorithm which is used to compute the angle of arrival (AoA) of the sources. An ADXL345 accelerometer provides information about board orientation to determine if the board has been knocked over by wind or an animal. The light sensor ISL 29023 can be used for power management part of the system. The EMS system also comes with an MTK339 GPS module and a DS1338 Real Time clock (RTC) which are used for node localization and Time synchronization. The RTC is first configured by the GPS module to acquire the time in UTC format through the satellites. The RTC is then periodically synchronized to the error precision of the GPS module (10 ns for MTK3339) just in case to prevent the effects of clock drift. The RTC is used to time-stamp the acoustic events. The GPS will also provide accurate (to within 3 meters or 50 meters depending on how much signal interference is present) information about the node location. Additionally, these in-situ measurements can be used to estimate the speed of sound depending on temperature and wind velocity profiles used in the beamforming algorithm to obtain more accurate AoA estimates.

2.3 Software Organization

It is extremely important that the software written for any complex hardware in an embedded system be really efficient for optimizing the power utilization while maximizing the performance of the system. Hardware/software co-design methodologies employed in the building of EMS focuses on this requirement. The $1/3rd$ octave filter bank, the sensor drivers for the onboard GPS module, the drivers for the two communication system expansion modules (GSM and XBee) and the fixed interval timer are parts of the programmable logic of the system. That is, the hardware for these components are explicitly coded in VHDL. The logic for the SCST algorithm, sensor suite, communication system and also the sensor drivers for the analog sensor suite are all written as a part of the processing system, MicroBlaze softcore processor of the ARTIX-7 FPGA. After building the custom logic and interfacing the custom hardware with the MicroBlaze and its peripherals, a bit-stream is generated. This bit-stream is then used to create a board support package which comprises of all the generic code and the libraries to support the hardware. The MicroBlaze is configured to have 512KB of instruction and data caches, which happens to be the maximum allowable cache memory for the MicroBlaze soft-core processor in the ARTIX-7 hardware. The available cache memory is more than enough for the processor to execute the firmware efficiently.

2.3.1 Interrupt Controller Design

In total, the peripherals in the EMS system generates nine hardware and software interrupts to the softcore processor MicroBlaze. The MicroBlaze module handles all these interrupts through an interrupt controller. The interrupt controller governs the way in which the system can function optimally without any of the interrupts interfering with the system functionality. Hence, the interrupt controller in a way is the core of the MicroBlaze software. The 9 interrupt sources in the EMS system are : a) 1/3 Octave filter bank, b) Debug port (UART), c) Record Toggle (push button), d) XBee Uart, e) GSM Uart, f) GPS Uart, g) IIC Bus, h) GPS Hardware Unit and i) Fixed Interval Timer .

In the EMS system, the $1/3rd$ octave filter bank generates a valid input for energy levels for each frequency band it outputs and all these valid bits are stored in a 33-bit wide register. When all the bits in this 33-bit register are high, the filter bank generates an interrupt. This interrupt signal occurs every second. The processing core of SCST algorithm is activated only after this interrupt occurs. The record toggle interrupt occurs when the user pushes a record button. This interrupt handles the functionalities such as creating and opening the relevant files in the SD card and writing data into them and also closing the file when the record operation is complete. The XBee and GSM communication systems are interfaced with the FPGA through UART. Both communication systems generate an interrupt signal as soon as they have data at their respective transmission and receive ports. It is essential that all the peripherals operate in the interrupt mode as opposed to polled mode because in the polled mode, the processor checks the Tx (Transmission) and Rx (Receive) ports of the peripherals irrespective of whether there is data present or not and this causes unnecessary power consumption. The drivers and the interrupt receptors for the onboard GPS module are written in the register transfer logic (RTL) using VHDL. As soon as the GPS module starts receiving a signal it will start sending interrupts once every second. The GPS UART module then receives the serial data from the Tx port of the GPS module and it sends an interrupt to the MicroBlaze and this interrupt lasts until the whole string of data is received. The inter-integrated circuit (IIC) bus also generates an interrupt when it is trying to configure (IIC write) the sensors and when it is trying to read (IIC read) from the sensor suite. There is also a Fixed interval timer built into the system. The reason why this timer is necessary is that the reporting of the events to the park station is done only a few times per day. In the current implementation, the data is reported once every 3 hours. So, this module generates an interrupt once every 3 hours. The fixed interval timer can very easily be re-configured within the microblaze block design to adjust the frequency of data reporting. Finally, there is also a debug port which interfaces with the FPGA through UART, that was embedded just for the purposes of debugging the FPGA software configuration of the EMS system.

It is straightforward to understand that these interrupts play a vital role in the operation of the EMS. So, assigning proper priorities to each interrupt is very crucial, without which the system will never function as planned. The record toggle interrupt is generated by the user by pushing the record button available on the board. This interrupt is given the least priority due to the fact that the interrupt line will stay high as long as the recording operation is not fully accomplished (files are closed), which happens by pushing the record button for the second time. Thus, if the record toggle interrupt is assigned a higher priority, this interrupt will always occupy the interrupt lines of the MicroBlaze causing the other interrupts to never occur, which will result in system failure. The record toggle interrupt is explicitly enabled every second in an infinite loop to make sure the other interrupts don't turn off this interrupt which might otherwise result in relinquishing control over file writing and storing the data in the SD card, causing permanent data loss. The interrupt that is generated from the $1/3rd$ octave filter bank occurs every second, i.e, it also is the most frequently occurring interrupt. The second most occurring interrupt in the EMS is generated from the GPS hardware unit. From the time that the antenna starts receiving the signal, the GPS hardware unit generates an interrupt every second. It can be clearly understood that, if these interrupts were given the highest priority, they would always stall the other interrupts and the comm systems or the sensor suite will never get a chance to communicate with the processor. For this very reason, the $1/3rd$ Octave filter bank and the GPS hardware unit have been assigned the least priorities after the record toggle interrupt. However, just like it was done with the record toggle interrupt, it is essential to enable the interrupt from the filter bank every second in an infinite loop to make sure that the data acquisition and the execution of the SCST algorithm does not collapse due to the overpowering of certain other interrupts. The debug UART has been given the highest priority in the interrupt controller. This is because this interrupt never occurs unless we are trying to debug the software with a computer, making it the least occurring or in fact a non-occurring interrupt while the EMS is deployed. The second highest priority is given to the second least occurring interrupt in the system, which

happens to be the fixed interval timer. The interrupt for this timer occurs once every three hours and all the sensor data acquisition and the communication system deployments are tied to this interrupt. Hence, it is very crucial that this interrupt gets the highest priority when the board is deployed in the field. The IIC bus is assigned the third highest priority because it has multiple sensors interfaced with it and it needs to communicate with all the sensors and wait until they respond. If the interrupt control from the IIC bus is relinquished by any other higher priority interrupt, there is a possibility that the whole system will enter an infinite loop where the software will be stuck in one place trying to read from the sensor which is not able to send data on to the IIC bus because the interrupt lines are occupied by the other higher priority interrupts. To make sure that this problem does not occur, the code is written in such a way that the other higher priority interrupts never occur when the IIC bus is operational. In this case, it is the fixed interval timer whose interrupt always occurs before the occurrence of IIC bus interrupt. The other interrupts are the XBee Uart, GSM Uart, and the GPS Uart. It is essential to make sure that among these, the GPS Uart is given the least priority because that occurs more frequently in comparison to the GSM and XBee. Among the XBee and GSM, the priority order is really not that important as they never will depend on each other.

Advanced eXtensible Interface (AXI) Interrupt Controller (INTC) [25] which is inbuilt in the Vivado IP catalog manager is the chosen interrupt controller for this system. All the interrupts of the system are first concatenated into a vector of 9 bits. This 9 - bit vector is then given as an input to the interrupt controller module. According to the Xilinx interrupt controller module, the interrupt that is associated with the least significant bit (LSB) always gets the highest priority and the interrupt associated with the most significant bit (MSB) in the vector will always get the least priority. The interrupts are arranged in the following priority order : 1) Debug port (UART), 2) Fixed Interval Timer, 3) IIC Bus, 4) XBee Uart, 5) GSM Uart, 6) GPS Uart, 7) GPS Hardware Unit, 8) $1/3rd$ Octave Filter Bank and 9) Record Toggle (Push Button) .

2.4 EMS Operational Overview

The operational diagram of the EMS system is shown in Figure 2.6. As soon as the system is powered on, the EMS system will start acquiring the acoustic data and generating the $1/3rd$ octave spectral features while simultaneously looking for sources of interest. There is also a provision for recording all the necessary data on to an SD card simultaneously while performing detection and classification by pushing the record button. The SCST algorithm [17] which is implemented on the Microblaze softcore processor, first performs sparse coding by using fast Orthogonal Matching Pursuit (OMP) [26] technique. The sparse coded data is then sent to a discriminative four level quantizer [17] - [27] to reduce the number of possible states. The conditional probabilities of the quantized vector given the previous observations are computed under each source and interference model using a Bayesian network [19]. The log-likelihood ratios are then computed and added to their respective sums. This result is then compared to a predefined threshold for making decisions. If the log-likelihood ratio value is greater than this threshold value, then the source is detected. For quiescent detection, the log-likelihood ratios are computed and accumulated for each source of interest. If the value of the log-likelihood ratio is greater than a pre-set threshold γ, then the end of the source is detected and the source is classified. After that, the cumulative ratios are set to zero and then the algorithm starts to look for a new source. For more detailed description, the reader is referred to [8], [17]

There are two counters currently set in the MicroBlaze firmware which counts up when a source is detected. When the processor sees an interrupt from the fixed interval timer, the processor will start querying the sensor suite for the values of pressure, temperature, etc and waits until there is a GPS signal lock. Once the GPS signal is locked, the system will first configure the RTC with the help of satellite data acquired by the GPS module to make sure that the time-stamping of the events are accurate at all times. Then, the software prepares a string in a format that is readable by the Structured Query Language (SQL) database hosted by an online server. This string contains information about the

system node localization (GPS coordinates), node ID, all the sensor values, the information pertaining to the number of classified sources (example: Jets and Helicopters). Once the string is prepared, the data is either sent directly to the cloud platform (if the module has a cellular connection) or it routes all the data to a gateway in the network with the help of the XBee transceiver. The source count values are then reset and the fixed interval timer is turned off. During this process, which typically takes about a few hundred milliseconds, the system is not able to do any detection and classification. Once this operation is completed, the detection and classification operation will resume again. All the signal labels are stored in a file in the SD card and the data can still be retrieved, just-in-case, the communication system should malfunction. The SD card slot of the EMS system has a capacity of up to 32 GB, which is a lot of storage space to dump $1/3rd$ octave data and the classification results. One need not worry about filling up the SD card completely for up to several weeks or even months.

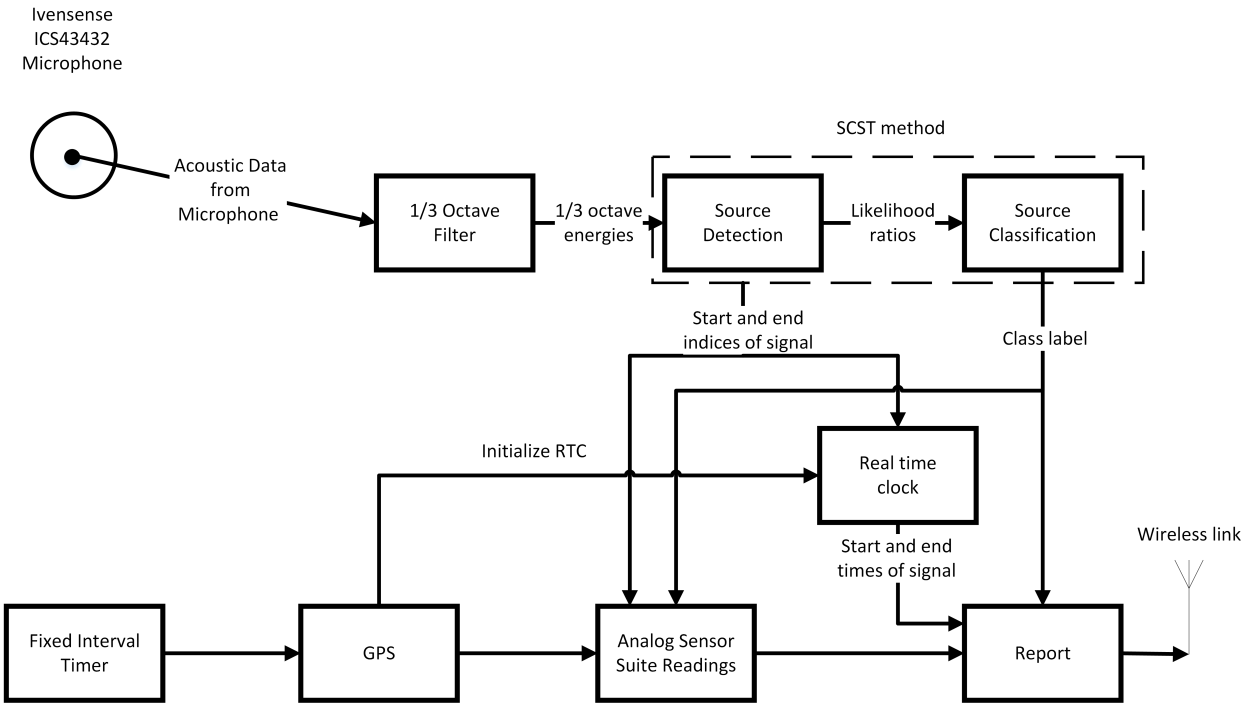

Figure 2.6: EMS Operational Overview.

2.5 Conclusion

EMS system is a powerful extension to the existing acoustical monitoring technology which typically uses expensive sound meters and microphones. The features that are present in the EMS make it possible to perform onboard detection and classification without any human intervention. The currently used Larson Davis method requires deploying the system in a remote area and then retrieve it to manually process the $1/3rd$ octave data. This is done by an expert using visual evaluation of the $1/3rd$ octave spectral data and then classifying the sources of interest. EMS system, on the other hand, automatically records the acoustic data, performs $1/3rd$ octave decomposition, detects and classifies the sources, and wirelessly reports the events every few hours. EMS system can be used to form a mesh network and work with other nodes for more accurate generation of noise map in national parks. However, when using a large number of EMS nodes, there are practical issues such as routing latency, packet losses and excessive flooding of packets that are bound to happen especially when the source to destination path is longer than one hop. These considerations limit the number of XBee nodes to a few hundred in order to maintain a reliable operation.

It must be pointed out that in comparison to the Larson Davis system the $1/3rd$ octave filter on the EMS uses a bank of digital filters as opposed to analog filters which don't suffer from quantization problems. However, the SCST algorithm works on sparsely coded and quantized data [17], hence these quantization effects may have little impact on the final detection and classification results. The application of EMS need not be limited to just the detection and classification of airborne vehicles. The hardware and software of the FPGA core can be reconfigured for different applications including: a) detection, classification, and tracking of ground vehicles for surveillance, traffic monitoring, and border control; b) gun-shot detection and location finding for both indoor and outdoor settings; c) detecting and localizing poachers, etc.

CHAPTER 3

DESIGN AND ANALYSIS OF ONE-THIRD OCTAVE FILTER BANK

3.1 Introduction

The purpose of the one-third ($1/3rd$) Octave filter implementation is to be able to generate $1/3rd$ spectral sub-band sound data on the EMS system. The data that is generated from the filter bank module is then used by the onboard processing system (MicroBlaze) to make detection and classification decisions. A spectral band is said to be an octave when the highest frequency of the sub-band is twice the value of the lowest frequency in that sub-band. Similarly, a spectrum is said to be a $1/3rd$ octave spectrum when the upper-edge frequency in the sub-band is equal to lower-edge frequency times the cubed root of 2 [28]. For the purposes of this application, the iterative filter bank [20] implemented on the EMS board splits the entire audio spectrum into 33 frequency bands or 11-octave bands where each octave band has three sub-band frequencies or $1/3rd$ octave frequencies. The $1/3rd$ octave filters have been implemented on the ARTIX-7 FPGA as a custom hardware unit so that the full advantage of computational parallelism that is available on the FPGA can be exploited.The filters that are designed meet the ANSI.S11 standards and are IEC class 0 compliant [28]- [29] . The implemented filters are 8th order digital infinite impulse response (IIR) Butterworth filters, which are obtained by cascading four second order IIR sections.

This chapter aims to provide a description of the design strategies employed in the implementation of the $1/3rd$ octave filter bank explained in Section 3.2. In Section 3.3 effects of quantization have been analyzed for the Direct Form II implementation of the $1/3rd$ octave filter bank. Section 3.4 discusses some of the issues related to the quantization noise in the

upper band filters associated with the Direct Form II structure and ways to correct it by using a Lattice-Ladder implementation of the $1/3rd$ octave filter bank.

3.2 Iterative $1/3rd$ Octave Filter Bank Implementation - An Overview

In an ideal situation, in order to split the spectrum into 33 sub-bands, we would need to apply 33 filtering operations. However, to reduce the number of resources needed for the implementation, the specification has been achieved iteratively by making use of only one second-order Direct Form II (DF II) IIR Butterworth filter. The iterating effect is achieved by cascading four second-order sections (SOS) to achieve a $8th$ order filter. The other $1/3rd$ octave frequency components in the octave spectrum are then obtained by just switching the coefficients of the same filter by the use of a finite state machine. From the properties of multirate systems, it is known that, downsampling a signal by a factor of N in the time domain, stretches its spectrum in the frequency domain by a factor of N. The higher frequency components present in the downsampled signal are aliased and need to be removed through low-pass filtering prior to processing it in the filter bank. Hence, by just downsampling the data by a factor of two for up to 11 times during successive iterations, one is able to sweep through the whole audio spectrum and split it into 33 sub-bands. The multi-rate filter bank architecture that is used to achieve this functionality is shown in Figure 3.1. In this figure, SOS corresponding to the first row is associated with the anti-aliasing low-pass filter, the second row corresponds to the band-pass filter in the upper band, the third row corresponds to the band-pass filter in the middle band and the fourth row corresponds to the band-pass filter in the lower band. Each row in the Figure 3.1 has four SOS's, implementing an 8th order filter. The sampling rate switching is controlled by a finite state machine in the code, which also handles the switching of coefficients to extract the samples in the upper band, the middle band, and the lower band, respectively. The sampling rate is initially set to the highest value of $50kHz$ and once the filtering is done in the higher, middle and lower bands

at the highest sampling rate, the state machine then downsamples the input and then the input is bandlimited by using a low-pass filter to remove the aliasing effects which occur due to downsampling and the process is repeated. The Multi-rate Timing block shown in the Figure 3.1 contains the logic for filter selection by sending the appropriate select line bits to the multiplexer module and also the logic for sampling rate reduction. The Multi-rate Timing block implements 11 rates in total, and at each rate, the input is downsampled by a factor of 2.

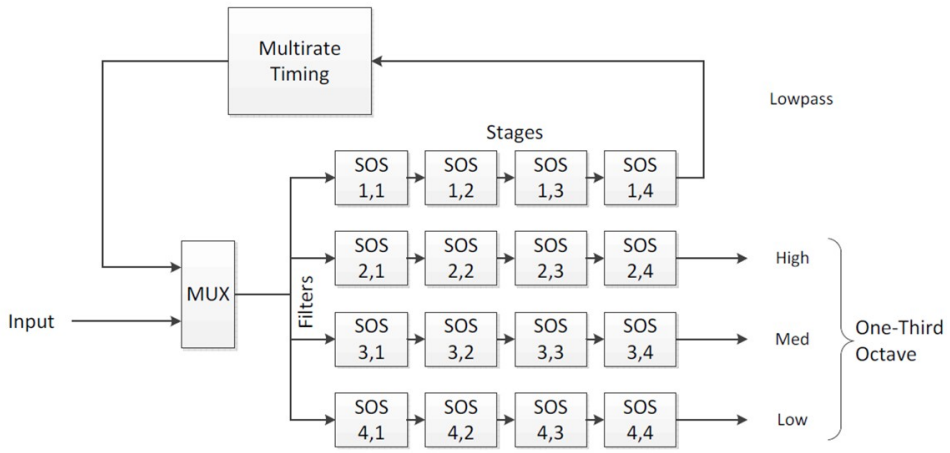

Figure 3.1: Multi-rate Filter Bank Architecture.

Figure 3.2 shows the time interleaving scheme employed in the $1/3rd$ octave filter bank design [20]. Each colored box represents one-time step. Since the filters are operating at a frequency of $50kHz$, each time step is $20\mu s$. The marked box indicates that the corresponding octave was executed during that time step. It can be noted from Figure 3.2 that the highest octave bands are executed in every time step, the second highest octave in every two time steps, the third highest octave in every four time steps, the fourth highest octave in every 8 time steps, and so on. Hence, the last octave or the 11th highest octave which corresponds to the lowest sampling rate is executed every 2^{10} time steps. It can also be noted that during each time step two octave bands or six $1/3rd$ octave bands are computed. The Multi-rate Timer block in Figure 3.1 first also decides the octave that needs to be executed during each

time step and then executes the filters corresponding to those octaves. The upper, middle and lower band associated band-pass filters within each octave are executed by choosing the appropriate coefficient inputs. The choice of switching the coefficients is made by keeping track of the number of clock cycles. This is done in VHDL by tracking this information in a counter array which is 4 bits wide and 6 bits deep. The reason why this array is 4 bit wide is that the first two bits keeps track of the individual second-order section (four) while the last two bits keep track of the number of stages in each $1/3rd$ octave band (four). The four stages in each $1/3rd$ octave band are the three band-pass filters corresponding to the upper, middle, lower sub-bands in that octave and the fourth stage corresponds to the anti-aliasing low-pass filter. The counter array is 6 bits deep to account for the fact that, during each time step, six $1/3rd$ octave filters or two-octave filters are executed.

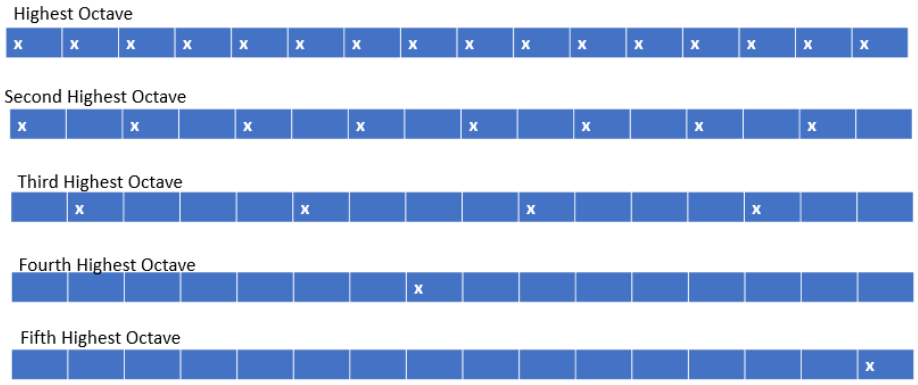

Figure 3.2: Timing Interleaving Scheme.

The Direct Form II implementation of a single section is shown in the Figure 3.3. The current Direct Form II implementation has only 3 multipliers, 4 adders, 2 delay blocks and there is one multiplier to account for the gain factor. The filter coefficients of the Direct Form II filter are 35 bit wide. The reason for choosing 35 bits is to reduce the coefficient quantization effects. It can also be noted that the Direct Form II filter structure uses the smallest number of delay blocks which makes it the most suitable filter structure to be implemented on the FPGA because of its inherent low memory requirements. The transfer

function for the low-pass and the band-pass filters for each type is represented by,

$$H(z) = \prod_{k=1}^{4} H_k(z) \tag{3.1}$$

where $H_k(z)$ is given by,

$$H_k(z) = \prod_{k=1}^{4} \left(\frac{b_{0k} + b_{1k}z^{-1} + b_{2k}z^{-2}}{1 + a_{1k}z^{-1} + a_{2k}z^{-2}}\right) \tag{3.2}$$

where a_{1k}, a_{2k}, b_{1k} and b_{2k} are the filter coefficients for the low-pass and the band-pass filters. The filter coefficients A_1, A_2, B_1, B_2 in Figure 3.3 are related to those in (3.2), i.e.: $a_{1k} = A_1$, $a_{2k} = A_2$, $b_{0k} = G$, $b_{1k} = B_1G$, and $b_{2k} = B_2G$, respectively.

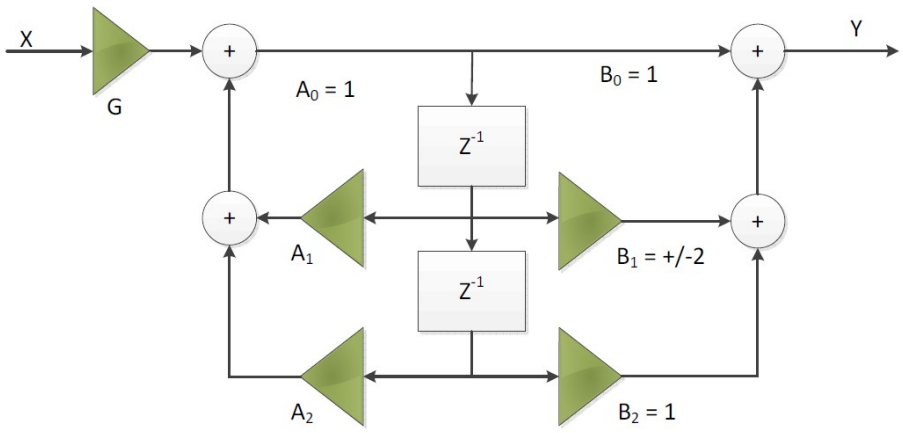

Figure 3.3: DF II Second Order Section.

The two delay blocks shown in Figure 3.3 are implemented in the FPGA by designing two 256 bit RAM modules with an 8-bit addressing scheme. As stated previously, the $1/3rd$ octave filter bank computes 6 $1/3rd$ octave time step. Hence, the RAM needs to be able to buffer six samples of data, with each sample being 35-bits. This is the reason why the RAM was designed to have 256 bits of memory. The delay elements are stored in this RAM by explicitly specifying a write address and this write address is a function of the current sampling rate, the filtering stage, and the current computational stage, where rate corresponds

to the sampling rate currently being used. The computational stage array explicitly keeps track of each filtering stage which corresponds to the band-pass filters in the upper, middle, lower sub-bands and the low-pass filtering stage. The computational stage is kept track of by using an array which is 6 bits deep and 2 bits wide. The reason for using 6 bits is that the FPGA computes the filtered output for 6 $1/3rd$ octave segments per time step. The 2 bits in each row of the array keeps track of all the four stages that are available in the filter bank. The filtering stage component is also an array that is 6 bits deep and 2bits wide. The filtering array keeps track of each individual second-order section in the band-pass filter modules of the $1/3rd$ octave filter bank. All the band-pass filters and also the anti-aliasing low-pass filter has four SOS associated with it and all the four second order sections can be tracked from the two bits that are available in the filter array. The computational stage array and the filter stage both ultimately functions of the number of clock cycles and these arrays are updated by using the counter array by referencing the appropriate bits and rows from the counter array. The information pertaining to the first two bits of every row in the count array is associated with the completion of each SOS and the last two bits are associated with each stage present in the octave band. A write address for the RAM is generated by concatenating the values of current rate and the appropriate bits in the filter array and the computational stage array. The read address for the RAM is also generated in a similar fashion by tracking the same components. The operation of coefficient switching is also performed by tracking the filter array and the computational stage array. The 3 coefficients A_1, A_2, B_1 and the gain factor G (from low pass filtering) of the Direct Form II filter shown in the Figure 3.3 are stored in the form of a 4×4 array and the fourth coefficient B_2 is hardcoded to unity. The coefficients are changed by indexing into these coefficient arrays by using the filter array and the computational stage arrays which ultimately are functions of the number of clock cycles occurred since a new sample was received. The first three rows in the coefficient array are associated with one of the upper, middle, lower band-pass filters of the $1/3rd$ octave sub-band, while the fourth row is associated with the anti-aliasing low-pass

filter. As an example, the coefficient array for the B1 coefficient in Figure 3.3 is expressed as,

$$\begin{bmatrix} 2 & 2 & 2 & 2 \\ 2 & 2 & -2 & -2 \\ 2 & 2 & -2 & -2 \\ 2 & 2 & -2 & -2 \end{bmatrix}$$

Figure 3.4 shows the generalized magnitude response of three band-pass filters. The normalized center frequencies associated with the upper band, middle-band and the lower band are 0.78π, 0.625π and 0.488π, respectively. Depending on the sampling rate, the actual value of these center frequencies will change for each octave.

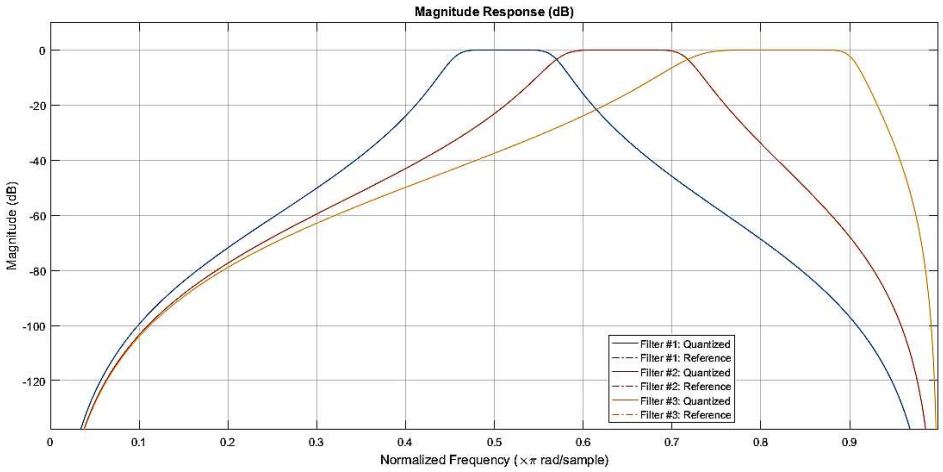

Figure 3.4: Magnitude Response of the 1/3rd Octave Filter Bank.

Once the filtering is performed for each of the 33 sub-bands in the $1/3rd$ octave spectrum, a valid bit associated with each of those is set to high. Since there are 33 sub-bands, a 33-bit wide register vector is maintained to keep track of the valid bits for all the sub-bands. The filter module produces raw output samples, each of which are represented by 35 bit wide fixed-point numbers. The filter output is then converted to 32-bit floating point format to obtain higher precision before energy is calculated for each of the 33 sub-bands in every one-second interval. Once the energy is computed, it is then converted to Sound Pressure Level

and expressed in dB ($SPLdB$). Note that the Effective Input Noise (EIN) of the microphone is subtracted from the energy value before it is converted to dB. This process is repeated across all the 33 sub-bands and for each sub-band and there is a valid bit associated with every calculated energy level. A 33-bit wide register vector is maintained to keep track of the valid bits for all the energy levels. Once all these valid bits are set to 1, the $1/3rd$ octave filter bank generates an interrupt to the MicroBlaze processor, which typically occurs once every second.

3.3 Quantization Error Analysis of DFII Structure

Here, we only consider the effects of product quantization since this is the most dominant source of error in digital filters. Additionally, the effects of coefficient quantization are almost insignificant and don't alter the location of poles and zeros of the transfer function enough to distort the frequency response of the system. This can be verified from the pole-zero location plots in Figures 3.5a, 3.5b, 3.5c for DFII-based IIR Butterworth digital filters and using a coefficient word length of 35 bits . The locations for the quantized and non-quantized pole locations are marked by '+' and '*' in these figures and it can be seen that they are nearly at the same spot in the unit circle. All the filter coefficients for this system were designed using fixed-point arithmetic instead of floating-point arithmetic as floating-point operations are computationally expensive. An analysis was done by designing the $1/3rd$ octave filter bank at various coefficient word lengths and it was found that 35 bits is the optimum word length at which the system produces a frequency response with minimal deviation from the ideal non-quantized version.

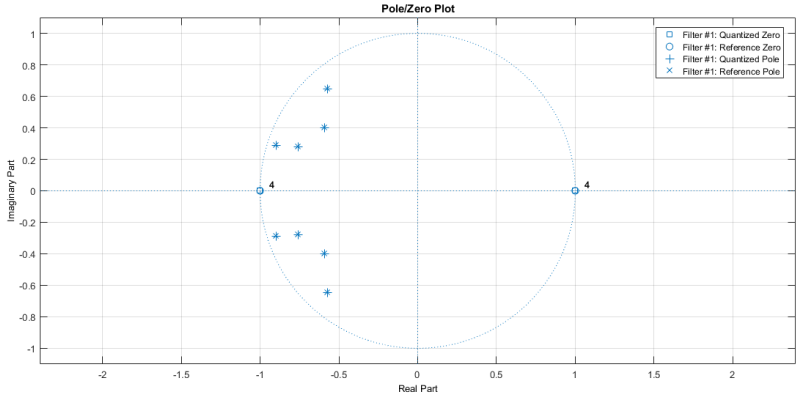

(a) Upper Band-Pass Filters.

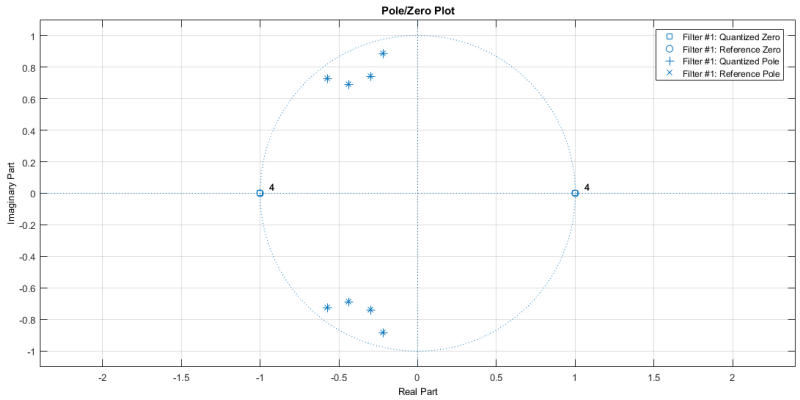

(b) Middle Band-pass Filters.

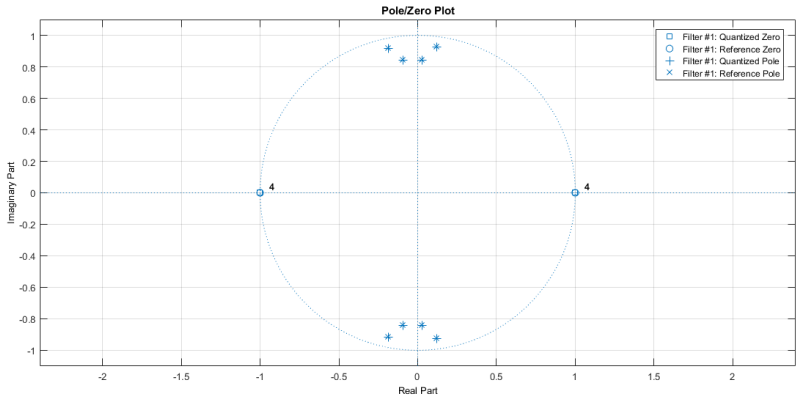

(c) Lower Band-pass Filters.

Figure 3.5: Pole-Zero plots for DFII Structure.

As mentioned before, the Larson Davis system uses analog filters and hence, do not suffer from quantization effects. As a result, we can use the $1/3rd$ octave spectrum generated by Larson Davis as a basis of comparison to analyze how much the $1/3rd$ octave spectrum generated by EMS is distorted due to the effects of quantization. A test was conducted in an abandoned airport in Fort Collins where a chirp signal from $250Hz$ to $2kHz$ was played through the speakers while both EMS and Larson Davis were placed approximately in the same location. The collected $1/3rd$ octave data is used to generate time-frequency plots for EMS and Larson Davis as shown in Figures 3.6a and 3.6b, respectively. As can be clearly seen, the Larson Davis system produced clean $1/3rd$ octave data while the data produced by EMS is slightly distorted since the energy values actually leak into adjacent frequency bands. As can be seen, the leaking effect is more pronounced in the higher frequency bands. This may be attributed to aliasing effects due to the folding of the spectrum caused by downsampling and the imperfections of the anti-aliasing low-pass filter which does not completely remove these effects. If this leaking effect becomes more prominent, the detection and classification accuracy could potentially suffer, despite the fact that the SCST algorithm uses quantized data after sparse coding to perform detection and classification.

Product quantization is observed at the output of every multiplier module in the digital filter. The outputs of these multipliers are used to generate a sum of the signal and the quantization error at each adder output. Product quantization is usually the most prominent type of quantization error. This is because, when two numbers each with a word length of B bits are multiplied, together the product could yield $2B-1$ bit result. But in order to maintain a constant word length of B bits, the $B-1$ LSB bits have to be truncated or rounded-off. This process can result in serious quantization errors, which is especially prominent for IIR systems because of the recursive nature. For a multiplier with coefficient b_i and input $x(n)$, the product quantization error $e(n)$ is defined as,

$$e(n) = b_i x(n) - Q[b_i x(n)] \tag{3.3}$$

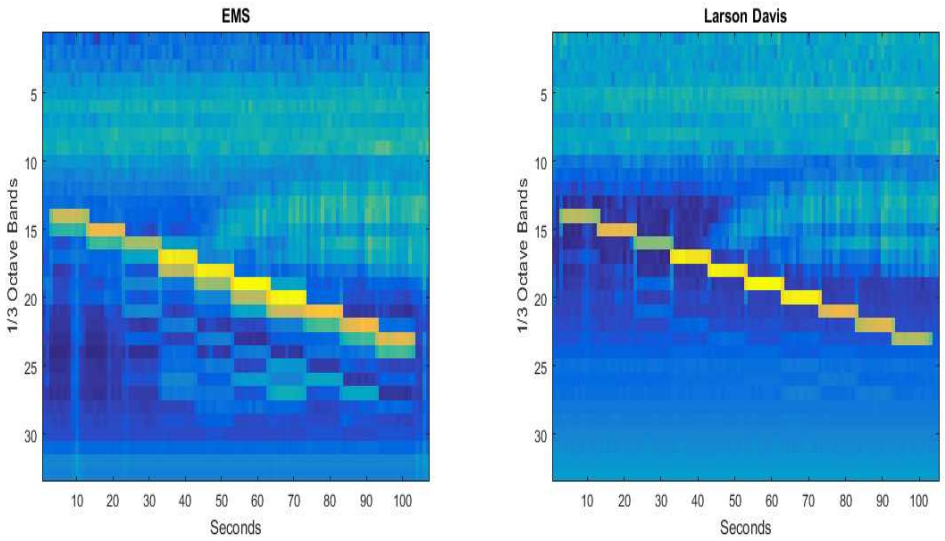

(a) EMS System. (b) Larson Davis.

Figure 3.6: Time-Frequency $1/3rd$ Octave Plots for both Systems.

where $Q[.]$ stands for the quantization process.

It can be easily verified [30] that the mean and the variance of $e(n)$ for round-off error are,

$$\mu_e = E[e(n)] = 0 \tag{3.4}$$

$$\sigma_e^2 = E[e(n)^2] = (2^{-2B})/12 \tag{3.5}$$

where $E[.]$ is the expectation operation.

It is also known that for a Direct Form II filter, the round-off noise power spectrum is given by,

$$S_{ff}(e^{j\Omega}) = \sigma_e^2 |H_{ef}(e^{j\Omega})|^2 + 2\pi\mu_f^2\delta(\Omega) \tag{3.6}$$

where $H_{ef}(e^{j\Omega})$ is the frequency response of the filter and μ_f is the mean at zero frequency given by,

$$\mu_f = \mu_e H_{ef}(e^{j0}) \tag{3.7}$$

Round-off error analysis is performed using DSP toolbox in MATLAB which uses (3.6) for Direct Form II filter implementation using structure used in the filter design to generate a round-off noise power spectrum. The noise power values observed at the center frequencies of the associated power spectrum at each sampling rate are used to form the basis of analysis in this chapter.

Figure 3.7 shows the plots of the upper band, middle band and lower band frequency filters and their round-off noise power spectrum values in dB at various sampling rates. It can be seen from this figure that the upper band filters are more susceptible to round-off noise compared to the lower ones. This can be due to imperfections in the anti-aliasing low-pass filter that are used to remove high frequency aliased components resulted from downsampling. The other reason could stem from the fact that the microphone only produces 24-bit samples which might not provide enough resolution to accurately capture the data. Another observation that can be made is that, as the sampling rate reduces, the round-off noise power values increase. It was seen from the Figure 3.2 that as the sampling rate reduces, the lower octaves are executed a smaller number of times compared to higher ones. That is, we have a smaller number of samples adding up to one second, thus it may not provide an accurate average power. Thus, the lowest center frequencies are the most affected ones.

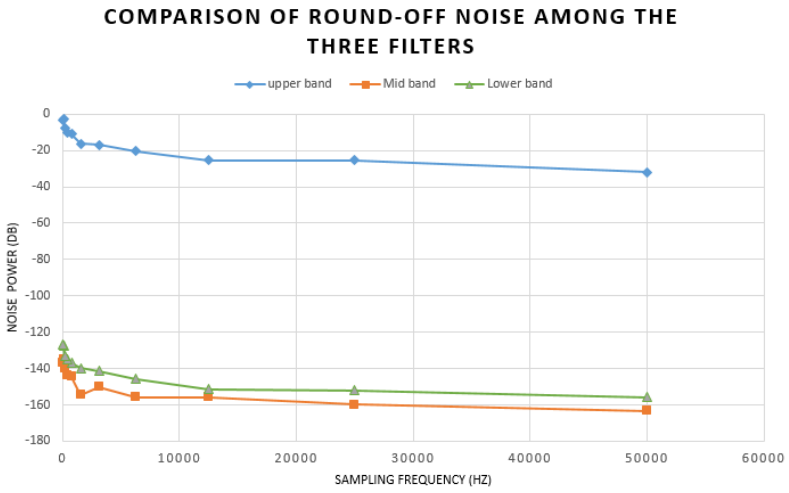

Figure 3.7: Direct Form II Quantization Effects in all the three filters.

3.4 Quantization Error Analysis of Lattice-Ladder Structure

It is clear from the analysis presented in Section 3.3 that at certain frequencies ($20Hz$ and $40Hz$) the quantization effects are very dominant, though the sources of interest do not lie in this frequency range. It must be pointed out that for the test results shown in Figures 3.6a and 3.6b, the lowest frequency considered was $250Hz$, and the round-off noise at this frequency was $-145dB$ which is fairly low and does not degrade the SNR enough to cause any detection and classification issues. The question is: Is it possible to improve the overall SNR of the $1/3rd$ octave spectrum and decrease the quantization effects considerably so that the EMS can operate nearly as good as the Larson Davis?. The answer to this question is yes, and the solution is $Lattice-Ladder$ architectures [31]. Prior research [32] shows that for fixed-point IIR filter implementation, the stability and frequency response of Lattice-Ladder structures are less prone to round-off errors. This would mean that we can implement the same filter bank with coefficients of smaller word length without causing significant round-off errors. Lattice-ladder structures are also shown [33] to have fewer limit cycle oscillations as compared to classical implementations. In this thesis, the Butterworth filter coefficients that were originally computed for the Direct Form II structure have been reconfigured to fit the lattice-ladder structure by using filter convert method readily available in MATLAB's DSP toolbox. This is done to make sure that our comparison is consistent and we can attribute the change in behavior solely to the filter structure and not any to any other design changes.

Figure 3.8 shows lattice-Ladder implementation of the same $1/3rd$ octave filter bank . Note that this figure only shows a part of the complete implementation (3 sections) out of the 8 sections for 8th order filter implementations. The word length of the filter coefficients in this implementation is chosen to be 24-bits as opposed to 35-bits in the case of Direct Form II considered before. Figure 3.9 shows the magnitude responses of the three band-pass filters for the lattice-ladder implementation of the $1/3rd$ octave filter bank. As can be seen from Figures 3.4 and 3.9, even at 24-bit coefficient quantization, the lattice- ladder architecture

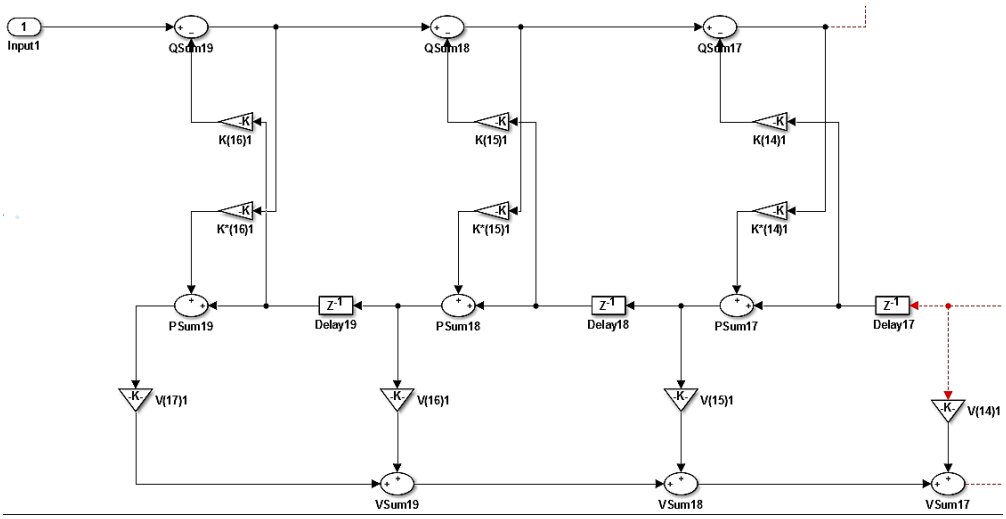

Figure 3.8: Lattice-Ladder Filter Architecture.

exhibits similar magnitude responses compared to the DF II implementation with 35-bit coefficient word length.

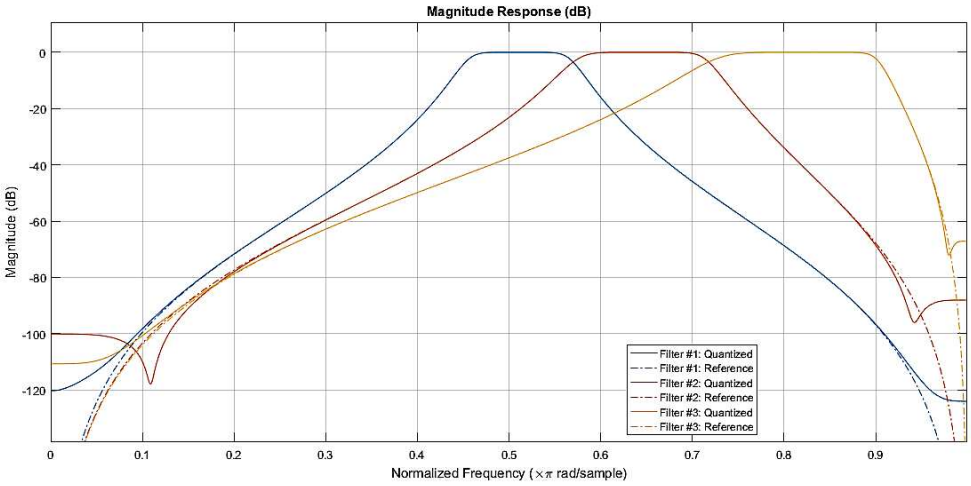

Figure 3.9: Magnitude Response of Lattice-Ladder Implementation.

For the sake of consistency, a similar quantization error analysis was done for the lattice-ladder filter realization by computing the round-off noise power at all the 11 sampling rates in order to compare the results with those of the 35-bit DF II implementation as shown in Figure 3.10. More specifically, the performance of both filter architectures is benchmarked at higher frequency bands with higher (for DFII) round-off error issue. Figure 3.11 gives a plot of the

noise power versus frequency, evaluated at higher frequency bands for both DFII and Lattice-ladder realizations. From these results, it is evident that the lattice-ladder implementation performs better and is much less susceptible to the quantization errors at these frequency bands. The noise power value at $20Hz$ and $40Hz$ for lattice-ladder architecture is $-60dB$ which reveals a significant improvement over Direct Form II-based implementation.

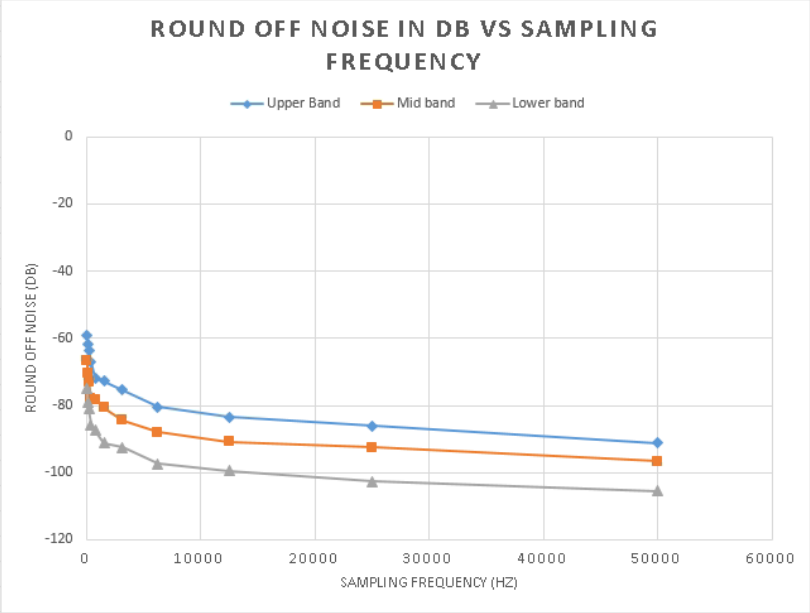

Figure 3.10: Lattice-Ladder realization Quantization Effects for all the Three Filters.

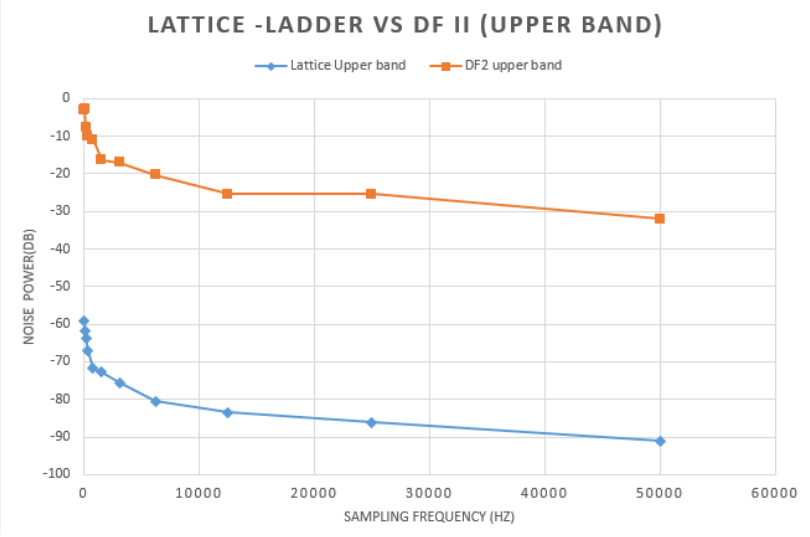

Figure 3.11: Lattice-Ladder implementation *vs* DF II implementation-Upper band Quantization.

3.5 Implementation Considerations for Lattice-ladder vs DFII

Group Delay: While the magnitude response of a filter gives the information about the signal output strength across the various frequencies, the phase component gives a way to measure the signal distortion that is, the rate of change of phase. Group delay, τ, is defined as the rate of change of phase, ϕ, with respect to the frequency, ω, which gives a measure of signal distortion,

$$\tau = -\partial\phi/\partial\omega \tag{3.8}$$

From Figures 3.5 and 3.13 we can see that the poles for both realizations are located at approximately same locations, while in case of DF II realization the zeros are located on the unit circle, so opposed to the zeros of Lattice Ladder implementation which are scattered all over the z-plane. This implies that both systems are essentially non-minimum phase systems. Hence, the group delay for both systems would not be minimized. Nevertheless, it can be noticed from Figures 3.12a and 3.12b that the group delay of the lattice-ladder architecture is about a few tens of microseconds versus that of the for Direct Form II which turns out to be a few tens of milliseconds. Moreover, the group delay in DF II realization is not constant for all frequency components as opposed to the lattice-ladder realization which exhibits a nearly constant group delay at all frequencies. A non-constant group delay usually translates to signal distortion. This might explain why the EMS system could not produce $1/3rd$ octave data as accurately as the Larson Davis system (refer to Figure 3.6).

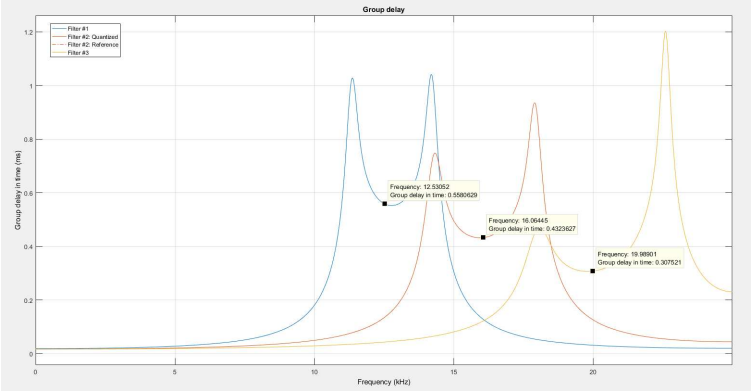

(a) DF II Implementation.

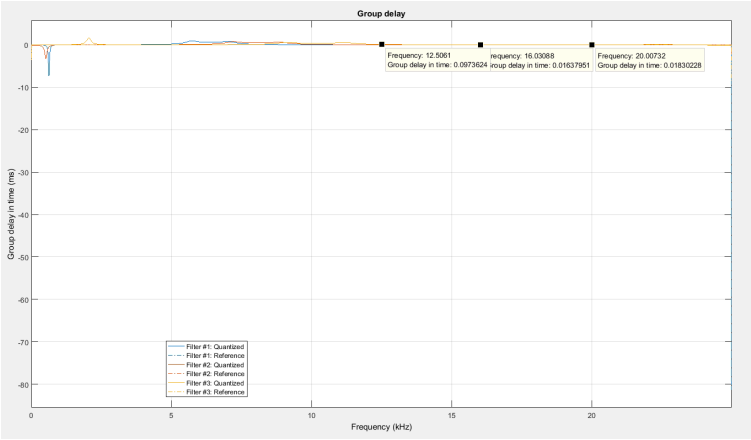

(b) Lattice-Ladder Implementation.

Figure 3.12: Group Delay for both Filter Implementations.

Hardware Implementation Complexity and Resource Consumption: When designing filters on the custom system on chips such as FPGAs, it is usually a standard practice to go with the DF II structure with cascaded SOS's when it comes to IIR filter design. Moreover, implementing DFII filter on the hardware through RTL coding is fairly straightforward and simple. The main reason is that it is easily scalable to higher orders while keeping the resource requirements constant. Whereas, lattice-ladder implementation is significantly more complex to code if we do not break the filter into sections and modularize it. The caveat here is that we need to accurately know what poles and zeros to pair up when we modularize lattice structure to make sure that the frequency response is not distorted

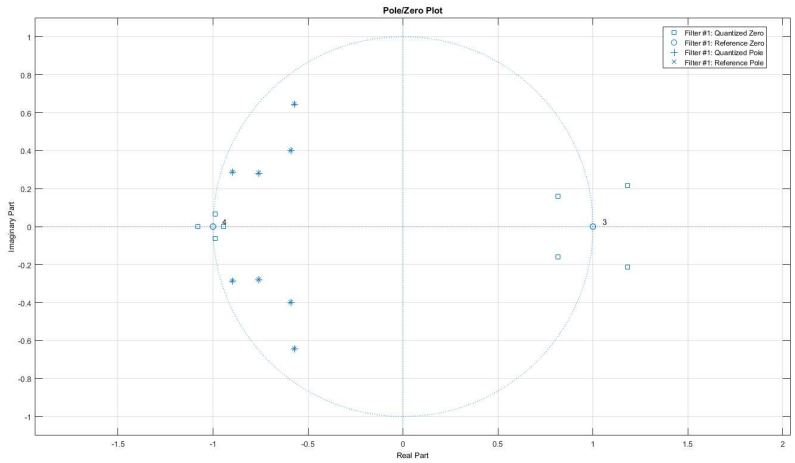

(a) Upper Band-Pass Filters.

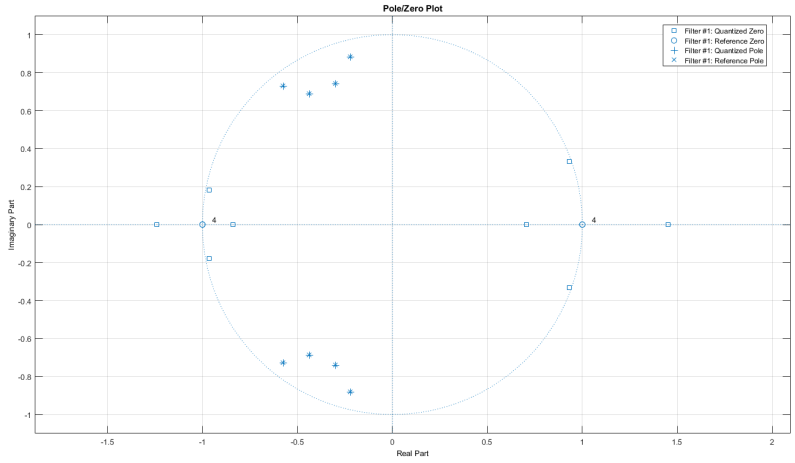

(b) Middle Band-pass Filters.

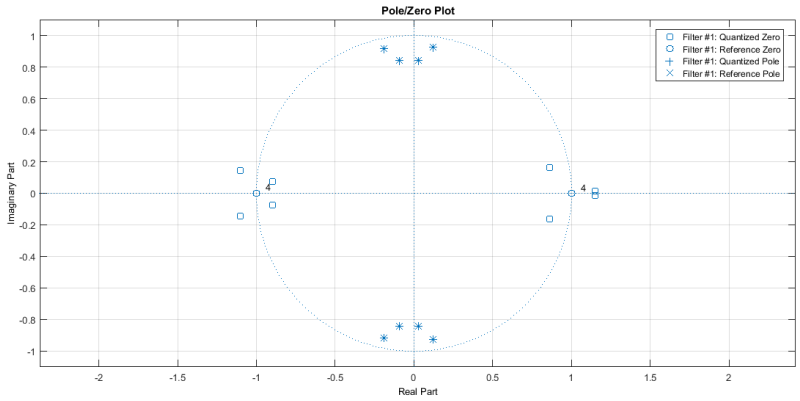

(c) Lower Band-pass Filters.

Figure 3.13: Pole-Zero Plots for Lattice-Ladder Structure.

and the stability is not compromised. This is actually a laborious process. Referring to Figures 3.13a, 3.13b, 3.13c, it can be seen that this could be a challenging problem to properly accomplish for all the octaves in our hardware as the zeros are scattered all over the z-plane.

Table 3.1: Implementation Cost in terms of Resources for 8th Order IIR Filter

Filter Structure	Number of Adders	Number of Multipliers	Number of Delay Blocks
DF II	4	43	2
Lattice-Ladder	23	24	8

Additionally, lattice-ladder realizations inherently consume more resources than other traditional forms of filter realizations on the FPGA [32]. From Table 3.1 it can be seen that for 8th order filter implementation, lattice-ladder filter uses a significantly higher amount of resources compared to DFII realization, which can pose scalability issues. Higher resource utilization usually translates to higher power dissipation and this can be undesirable in battery operated sensor nodes.

3.6 Conclusion

The $1/3rd$ octave filter bank implemented on the EMS system is highly resource efficient and capable of achieving high sampling rates. The filter bank is designed in such a way that the filter order can be scaled without causing significant hardware overhead. The analysis of quantization effects of the DF II filter structure indicated that the upper-frequency band-pass filters were more susceptible to quantization errors compared to other frequency bands. We also verified numerically that a lattice-ladder implementation of the $1/3rd$ octave filter led to less susceptibility to quantization effects compared to the DF II filter structure. However, was also noted that implementing a lattice-ladder filter bank is significantly more complex compared to the implementation of DF II on the FPGA. The higher amount of resource consumption and hence, higher power requirement makes it unsuitable for FPGA based environments. Moreover, as discussed in Section 3.3 the center frequencies that are more susceptible to quantization noise are $20Hz$ and $40Hz$. But, the acoustic signature produced

by the sources of interest is usually higher than $100Hz$ and any signal below this frequency is usually treated as interference and canceled out by the SCST algorithm. Thus, this issue is not likely to affect our detection and classification results.

CHAPTER 4

EMS COMMUNICATION SYSTEMS

4.1 Introduction

As mentioned in Section 2.2.1 one of the main features of the EMS system is its ability to autonomously report the classified events to the park station. EMS system is designed with two expansion slots: one for a cellular module and another for an XBee transceiver. This flexibility allows the EMS systems to use either the GSM module or the XBee radio and transmit data to a park station depending on the availability of cellular service in the deployment location and the distance between the deployment sites and the park station. It is important to note that only a few EMS nodes, known as the master nodes, will need to be facilitated with the GSM feature, whereas all the EMS nodes will have XBee communication facility. The nodes that only have XBee's mounted on them are referred to as slave nodes. The master modules act as gateways in the network. This communication scheme allows slave nodes to be deployed in areas with poor cellular connectivity so long as they are able to communicate to adjacent nodes using the XBee radios and route their data to a master node which has good cellular connectivity. The EMS Xilinx Artix 7(XC7100T)-based main board populated with the GSM and XBee expansion prototypes were shown in Figure 2.5.

This chapter focuses mainly on the design and analysis of the communication system for the EMS board. Section 4.2 focuses on addressing some of the terminologies related to the Zigbee protocol and Zigbee communication as applied to the EMS system. In Section 4.3 a mesh network consisting of six EMS nodes is simulated and an analysis is presented to evaluate packet losses in the network as a function of the distance between the nodes and also as a function of a node failure within the network.

Section 4.4 describes how the data is transmitted to the park station using the GSM module. Conclusions are presented in Section 4.5.

4.2 Zigbee Communication

XBee is a brand name for Zigbee's developed by Digi International. Xbee PRO is a high power version of the XBee which comes with a much higher transmission range and receiver sensitivity in comparison to standard XBee. The XBee module currently being employed in the EMS system is the XBee PRO S3B paired up with a 2.1 dBi (decibel with respect to isotropic) half wave dipole antenna [34].

Zigbee protocol can be understood by reviewing its four important layers : a) Physical layer (PHY), b) Media Access Control layer (MAC), c) Network layer and d) Application Layer as shown in Figure 4.1. The PHY and the MAC layers of the Zigbee are defined by the IEEE 802.15.4 Wireless Personal Area Network (WPAN) standards [35] while the Network and the Application layers are defined by the Zigbee Alliance [36]. IEEE 802.15.4 WPAN standards define two PHY layer formats, one for modules operating at $2.4GHz$ and the other for modules operating at $868/915MHz$. The $868MHz$ band is allowed only in Europe while the $915MHz$ band is allowed in the North American region for radio communication. From the literature it is known [37]- [38] that the path loss is proportional to the logarithmic inverse of wavelength. The modules operating in the $868/915MHz$ have more than twice the transmission range in comparison to the modules operating at $2.4GHz$ [38]. Hence, a Zigbee module which operates at $915MHz$ frequency was specifically chosen for EMS application. At the MAC layer, Zigbee uses Carrier Sense Multiple Access protocol with Collision Avoidance feature (CSMA/CA). In the CSMA/CA protocol, the packet transmission to the destination node is only performed when the communication channel is available. If the communication channel is occupied, the transmitter holds the packet for a random time frame defined as the backoff factor which is basically a down counter that has a pre-set maxima. The transmission channel is checked again after the backoff counter gets to zero and if the

channel is free, the packet is transmitted or else the backoff factor is re-adjusted and the whole scenario is repeated again until the channel becomes available. Once the packet is transmitted, the source looks for an acknowledgment from the receiver by waiting for a short time frame known as the receiver timeout. If the acknowledgment is not received within this time frame, the packet is assumed to be lost and a re-transmission is set up. It is to be noted that the transmission process will be initiated only if the destination node is within the transmission range of the source. Moreover, the Collision Avoidance (CA) feature of the MAC layer ensures that no two valid packets of the 802.15.4 format [39] are transmitted simultaneously to the same receiver. The transmission range at the MAC layer is defined by a factor known as Receiver Sensitivity [40]. Receiver sensitivity is defined as the lowest power at which the signal is distinguishable from the noise. This information is provided by the Zigbee manufacturer.

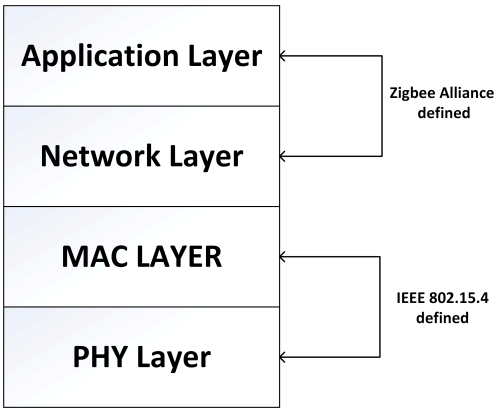

Figure 4.1: Zigbee Protocol Stack.

At the Network layer, Zigbee uses a routing protocol known as Ad-HOC On-Demand Distance Vector (AODV) [41]. In this protocol, the source to destination path is not fixed and the path is dynamically allocated during each transmission through a process known as route discovery. In this networking scheme, a routing table is maintained at every node that records all possible active paths from source to destination and also flags the nodes that are part of the active connection. The routing table also stores information about the destination address, next hop address, sequence number and the lifetime of the route. If the

route is not used for a certain period of time, the route expires and is removed from the routing table. During the process of route discovery, the protocol first checks if there is an up-to-date route to the destination, if yes, the packet is forwarded to the hop address that is indicated in the routing table. If the path from source to destination is not up to date, the sender broadcasts a special packet called the Route Request (RREQ) packet. This packet contains information about the source IP address, source sequence number, destination IP address, destination sequence number. Broadcasting is done through a mechanism known as flood routing [42]. In this mechanism, the sender broadcasts the packets to all its neighbors and each neighbor that receives the packet forwards it to its neighbors and this operation continues until the packet reaches the destination. The sequence number in the routing table is used to make sure that a packet is not forwarded more than once in the network. Sequence number also acts as a routing time stamp which helps determine an up to date path to a destination node. A higher sequence number signifies a more up to date path between source and destination. During the process of flood routing, the broadcast messages are only sent to the nodes that are a part of the active connection. An active connection consists of the nodes that were used for routing data from source to destination which is tracked by using a sequence number. This helps in conserving energy in the network by avoiding unnecessary forwarding of packets that can lead to more power consumption. This also allows for a faster detection of link failures in the network as the failure check messages are only sent to active nodes.

The Application layer of the Zigbee takes care of the message forwarding between nodes, address mapping from the MAC layer to the Network layer, initiating or responding to the binding requests and also takes care of packet fragmenting and reassembling. The two main application layer operating modes of the Zigbee are, Application Transparent (AT) mode and the Application Peripheral Interface (API) mode [43]. In AT mode, the wireless link acts like a serial line replacement and is optimal to be used when there are only two XBees in the network. When the XBee's are configured in AT mode, it is not possible for two

sources to send packets to the same destination simultaneously. The sources are required to be temporally synchronized in such way that the transmission overlap is avoided, which otherwise, can lead to loss of information. Moreover, the destination node needs to be re-configured before sending each packet, making it difficult to use AT mode in an XBee network. On the other hand, API mode is specifically designed so that communication between multiple nodes can be easily established without the worry of information loss. In API mode, instead of directly sending raw serial data over the air, the data is sent in the form of packets known as API frames. The frame consists of various fields as shown in Figure 4.2. The start delimiter field consists of a predefined data sequence (0x7E) which indicates the beginning of a data frame. The length field is used to denote the number of bytes present in the frame data field. The frame data field consists of the 64 bit MAC address of the destination device along with the actual payload. Lastly, the checksum field is used to evaluate the data integrity. In API mode, the packet source address can be easily identified as the received data includes the sender's address, that can be used to pinpoint node failures. Each received packet also contains the Receiver Signal Strength Index (RSSI) value, which helps in evaluating link quality.

Start delimiter	Length		Frame data								Checksum
1	2	3	4	5	6	7	8	9	...	n	n+1
0x7E	MSB	LSB	API-specific structure								Single byte

Figure 4.2: API Frame Packet Structure.

In the EMS system, the XBee is interfaced with the ARTIX-7 FPGA through a Universal Asynchronous Receiver Transmitter (UART) bus. The UART is configured to operate in the interrupt mode, which means that the processor will be stalled until the whole string of data is transmitted or received through the UART. The interrupt handler for the XBee UART consists of an event counter which counts up after each byte of data is processed by the UART. The interrupt is not released until a pre-specified number of bytes of data has been processed. The EMS system is configured to send the GPS coordinates, time stamps, the

sensor suite measurements, node ID and actual counts of the classified sources. The data is packaged in the string format. The range of possible values for the length of this string was experimentally determined to be between 120 to 128 bytes. The actual size of the string will vary depending on the sensor outputs. Since it is hard to predict the actual size of the string, the XBee UART is configured in such a way that it always sends and receives 128 bytes. If the actual length of the string is less than 128 bytes, the string is simply zero-padded and transmitted. This redundancy ensures that correct data is transmitted at all times. Since XBee's in the EMS are functional only a few times a day, the power consumed through transmission and reception of data through XBee does not contribute to the average power consumption of the board.

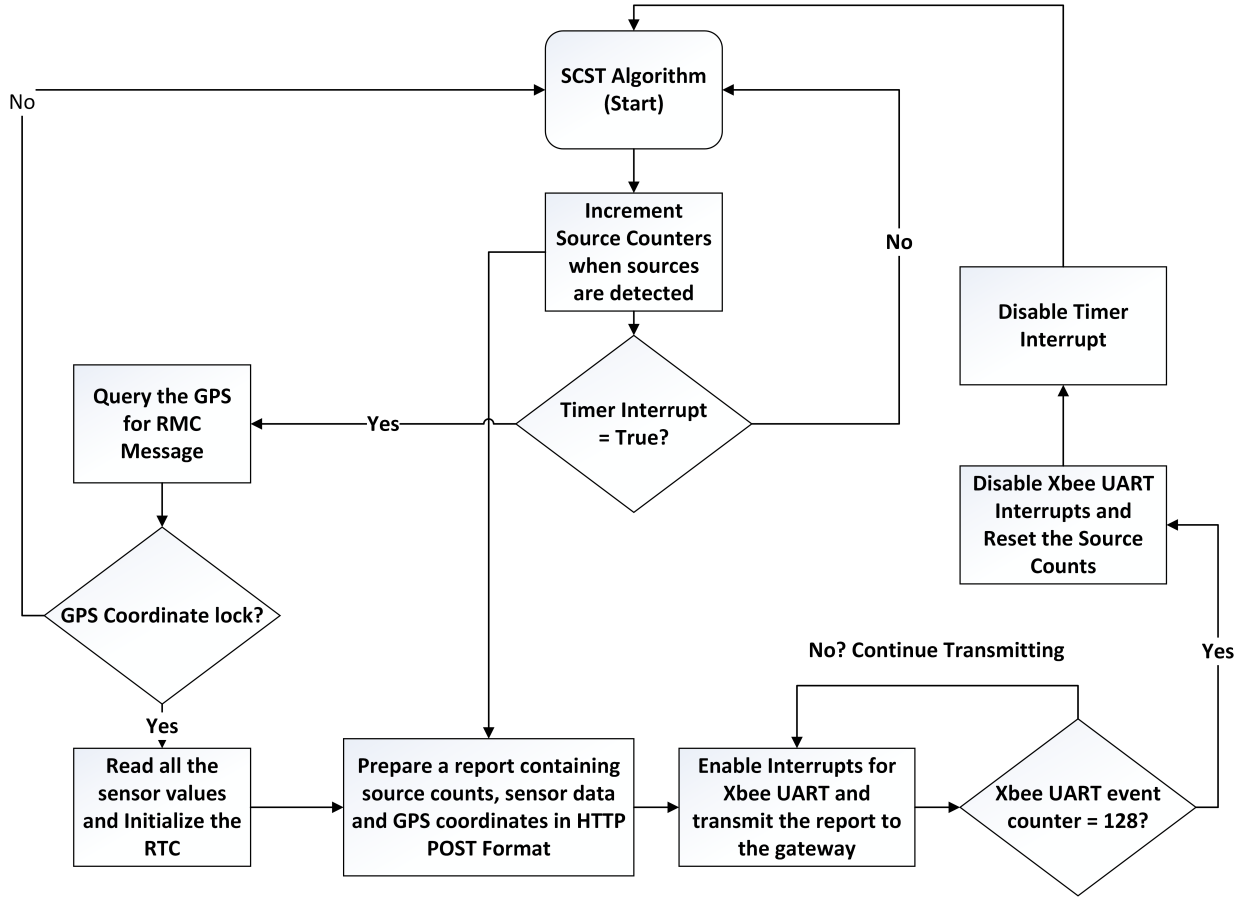

Figure 4.3: EMS Slave Node Operational Overview.

The operational overview of the communication systems of the slave module is shown in Figure 4.3. The actual counts of the sources of interest are tracked using two counters that are interfaced with the SCST algorithm in the MicroBlaze firmware. The current design reports wirelessly to the park station once every few hours. This transmission event is controlled by a timer interrupt that has been interfaced with the MicroBlaze softcore processor. Once the interrupt is triggered, the GPS module is queried for Recommended Minimum Configuration (RMC) data by sending a Proprietary MediaTek (PMTK) command to the GPS module through serial UART bus, which is a transfer protocol for Global Navigation for Satellite Systems (GNSS) designed by MediaTek. The queried RMC message contains information related to the latitude, longitude, the time stamp of the coordinate lock, date, and speed over the ground in knots. The obtained date and time information are used to initialize the onboard real-time clock (RTC). The coin cell battery that is present in the EMS system, is coupled with the RTC to make sure its values are always up to date , even when the board is not powered. It can be noted from Figure 4.3 that, the reporting process is not initiated unless GPS lock is obtained. This is because GPS is used to synchronize the RTC to get accurate timestamps of the source events and this is very important for the beamforming algorithm [22]. The softcore processor communicates with the IIC bus in parallel to read the outputs from all the sensors, including the barometric pressure sensor, PCB temperature sensor, accelerometer, 3-axis digital compass, light sensor and the battery gas gauge which outputs the actual amount of charge in coulombs that is present in the battery. In the SCST algorithm, two counters have been set up to keep a track of the number of events of Jet and Helicopter classes . The collected data is then packaged into a string along with a pre-specified node ID in a format that is compatible with the HTTP (Hyper Text Transfer Protocol) post method and the PHP (Hypertext Preprocessor) application script that runs on the server. Once, the XBee transmission is complete, the XBee UART interrupts are disabled and the source counts are reset to zero. The timer interrupts are disabled and the SCST algorithm will resume detection and classification.

4.3 XBee Mesh Network

At the time of writing this document, only two fully functional EMS nodes were built. Thus, it was not possible to physically build a mesh network and instead, a network of EMS nodes was built using a simulator to analyze packet losses as a function of the distance between the nodes. Additionally, intermediate node failure cases were introduced to understand their impact on packet losses. Network Simulator-2 (NS-2) [44] simulator was chosen to study the EMS network because of the substantial support it provides to simulate 802.15.4 modules and also due to its extensive use in literature to study wireless sensor networks. NS-2 is an open source simulator whose source code is written in C++. This allows the user to easily modify the source code of the routing protocols to suit the specifics of the system. NS-2 also allows the user to be very specific in defining the modeling parameters, including the antenna details , radio propagation models, and network traffic details. The simulator environment of NS-2 is based on Object-oriented Transaction command language (OTcl) [44]. These features make NS-2 a perfect choice to study the EMS wireless sensor network compared to other competitors.

In our simulation, a mesh network was constructed by considering six EMS nodes in the NS-2 platform as shown in Figure 4.4 where nodes are classified as Coordinator, Routers, and End device. This classification is done based upon the functionality of each node. The coordinators and the routers in the network are fully functional devices (FFD), meaning, they are able to transmit, receive and forward packets. The end device, on the other hand, is a reduced functional device (RFD) which can only send and receive data but cannot forward any packets. EMS end device, also known as the gateway, is equipped with both GSM and XBee functionalities and acts as a gateway to the park station. The end device is mostly asleep and only wakes up at certain times of the day to service other nodes in the network, making it suitable to operate on battery for a longer period of time. In a XBee network, there can only be one coordinator at any given time, which is responsible for initiating and forming the network. The coordinator acts as a parent node to the router nodes that are a

part of the active connection from source to destination. A router node is also an FFD much like the coordinator node, but it is mainly used to expand the network [45]. The routers are also responsible for allowing new nodes to join the network.

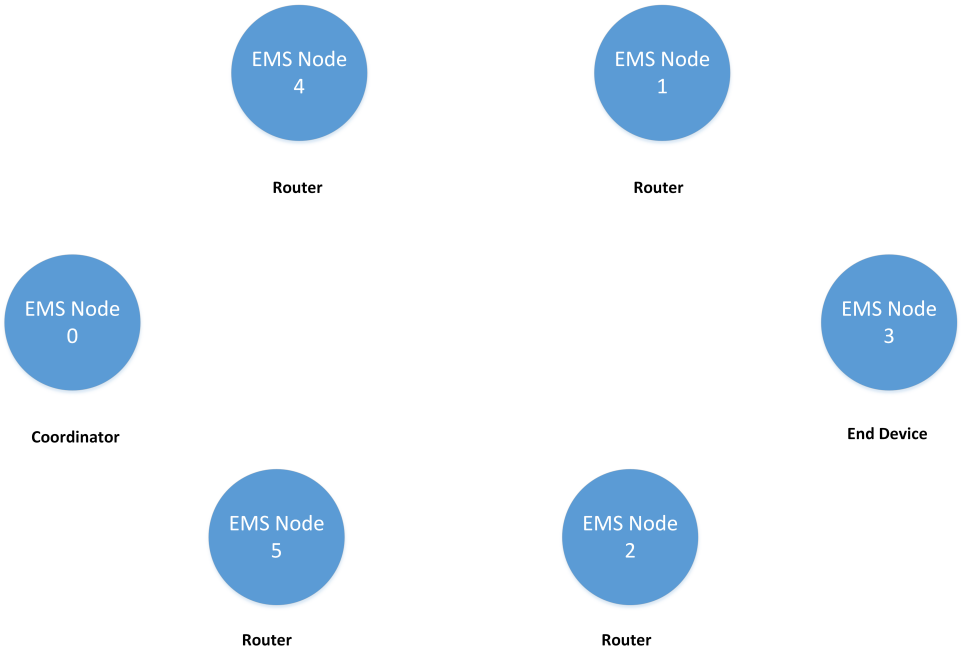

Figure 4.4: A Mesh Network of Six EMS Nodes.

4.3.1 XBee Range Test

The purpose of this experiment was to understand how the packet losses vary as a function of the distance between the nodes in the presence of interference and also to evaluate how they would change when a node close to the gateway fails versus when a node far from the gateway fails. In order to model the network as close to the real hardware as possible, the range of the XBees used in the EMS system was first assessed in an environment consisting of a fair amount of obstacles in the form of walls, trees, steel. The test was performed with two XBee modules, by connecting one of the modules to the laptop using the Future Technology Devices International (FTDI) XBee to USB adapter as shown in Figure 4.5. The other XBee module was connected to the EMS board. The XBee connected to the EMS board acted as the receiver while the XBee connected to the laptop was the sender. The data transmission

from the laptop to the EMS was set up by using XCTU software [46], provided by Digi International.

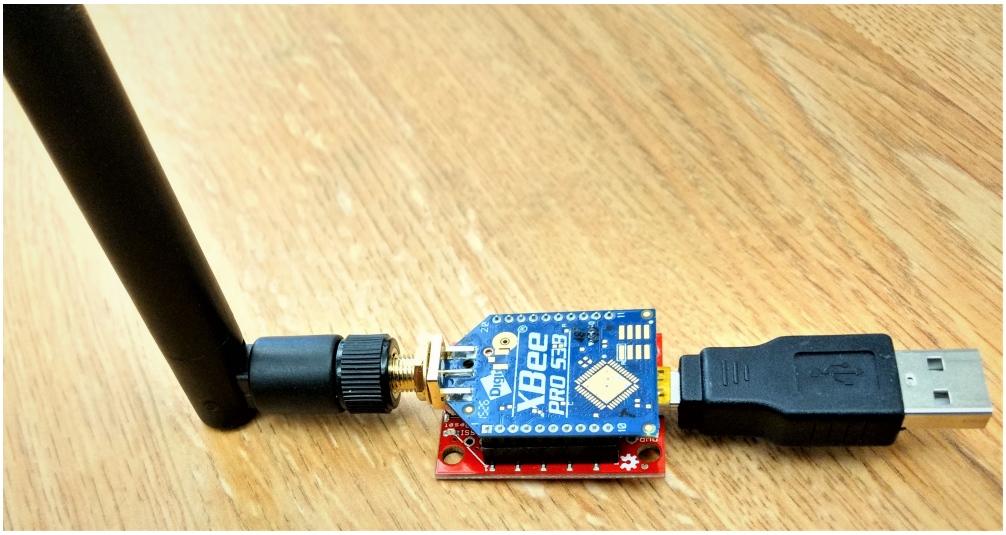

Figure 4.5: XBee with FTDI Converter.

The two XBees were first pre-configured to operate in AT mode using XCTU. The test configuration used in the XCTU software is shown in Figure 4.6. Cluster ID 0x12 was chosen as the range type test, where the destination node echoes transmitted packets back to the source as an indication of reception acknowledgment. Receiver (Rx) timeout is defined as the maximum time in milliseconds the source waits to receive an acknowledgment. This value is set as 1000 milliseconds. The Tx time is basically the time interval in milliseconds between successive packets and this is set as 4000 milliseconds to allow for sufficient trials of re-transmissions, in case of bad connectivity. The GUI in the XCTU software clearly displays the RSSI values and the packet loss percentages. The test was carried out by placing the two XBees 50m, 100m, 150m, 200m, 300m, 450m apart. The value of RSSI was noted down at each of these cases and is plotted separately as a function of the distance between the nodes in Figure 4.7.

It can be noted from Figure 4.6 that a packet was lost at an RSSI value of -60 dBm (decibel milli-watt). By referencing Figure 4.7, it can be roughly estimated that packet losses start occurring when the nodes are placed at 300 - 350m apart in a noisy environment

Figure 4.6: XBee Range Test Configuration.

constituting of trees, walls, ground etc. It must be noted that in this experiment, at each proximity several RSSI values were obtained by aligning the Xbee's at various angles other than the line of sight and also by hiding one of the modules behind a tree or a wall to induce shadowing effects. An average value of the RSSI measurements was then taken at each proximity. The two-ray ground radio propagation model in the NS-2 simulator requires the information about the receiver signal strength at all the node proximities to accurately model the transmission range of the XBees. Hence, the RSSI values measured from this experiment were used as a measure for range modeling in the simulator to create a more practical scenario.

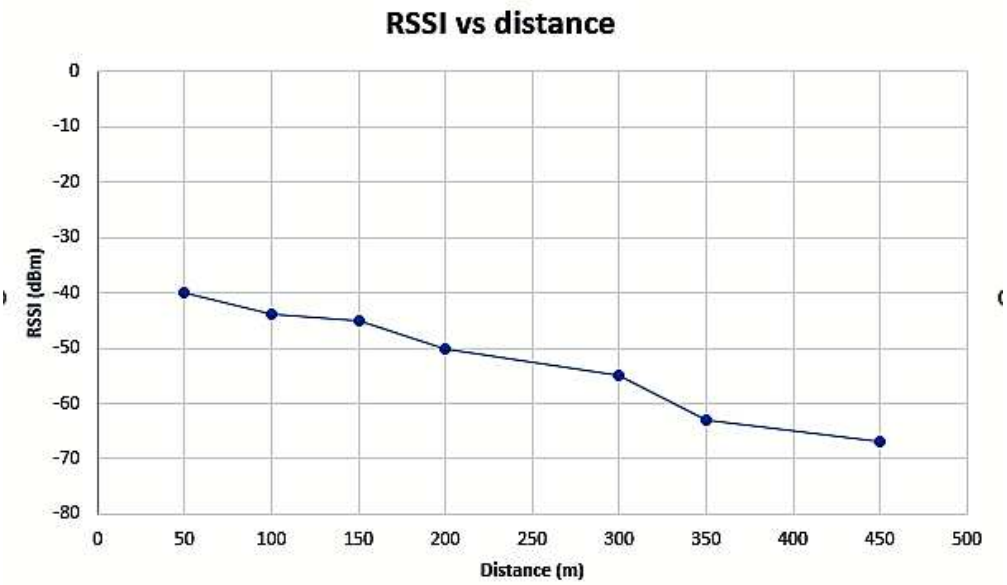

Figure 4.7: RSSI Variation with Distance.

4.3.2 XBee Mesh Network Simulation

The main purpose of this experiment was to understand the impact of router failures on the packet transmission reliability when data is sent from the coordinator to the end device. In this experiment, the source and the destination nodes were kept more than one hop distance apart and the packets were forced to go through routers to reach the destination. In a mesh network, there is often more than one path from source to destination, but this will not be the case when some of the nodes in the network fail due to various reasons like power loss or loss of line-of-sight. Hence, it is important to understand how the locations of node failures affect the packet loss percentage in the network.

The simulation was executed by specifying the details shown in the Table 4.1. The antenna that is coupled with the XBee PRO S3B module is a $2.1dBi$ half-wave dipole antenna, which in linear scale translates to a transmission gain of 1.6. A half- wave dipole antenna is an omnidirectional antenna, i.e., it has a spherical radiation pattern. The PHY and MAC layers are defined by IEEE 802.15.4 standards as mentioned in Section 4.2.

The NS-2 simulator supports three radio propagation models, namely, the free space model, the two ray ground reflection model, and the shadowing model. The free space and

Channel type	WirelessChannel
PHY	Wirelessphy/802.15.4
MAC	802.15.4
Radio Propagation Model	TwoRayGround
TwoRayGround System Loss factor	1
Antenna Type	Omnidirectional
Antenna gain	1.6
Operating Band	$915MHz$
Data rate	40kbps
Number of nodes	6
Routing Protocol	AODV
Max Packet size (Bytes)	128
Traffic Type	constant bit rate (cbr)

Table 4.1: Modeling Parameters

the two-ray ground reflection models assume that the antenna's radiation pattern is circular in shape, whereas, the shadowing model assumes distorted radiation patterns (elliptical in this case). The free space model assumes that there are no obstacles or interferences in the path between source and destination. Free space model assumes the communication range as a circle centered around the transmitter. If the nodes are within the circumference of the circle, the nodes receive all the packets, if not, the nodes lose all the packets. The received signal power $P_r(d)$ in free space at a distance d is calculated by using Friis equation [47],

$$P_r(d) = \frac{P_t G_t G_r \lambda^2}{4\pi^2 d^2 L} \tag{4.1}$$

where P_t is the transmitted antenna power, G_r and G_t are the transmitter and receiver antenna gains, respectively, λ is the wavelength of the RF carrier and L is the system loss factor. It must be noted that a ground level sensor network will never satisfy a free space since a significant fraction of the RF energy bounces off the ground, which results in reflection losses. The closer the antennae are to the ground, the higher are the chances of ground reflections and path loss. This can be understood by referring to the Okumura model [48]

for path loss, described by the equation

$$Pathloss \approx P_r(d) + A(f,d) - G(h_{tr}) - G(h_{re}). \tag{4.2}$$

where, $P_r(d)$ is the free space path loss, $A(f,d)$ is the medium loss as a function of distance and frequency, $G(h_{tr})$ and $G(h_{re})$ are the gain due to the height of the transmitting and receiving antenna from the ground.

The radio propagation model used in this experiment is the two-ray-ground reflection model. This model considers both the reflected path and a direct path between the source and the destination. Hence, this model gives a more accurate prediction of the link quality between the nodes. When using the two ray ground reflection model, NS-2 calculates the received signal strength $P_{TRG}(d)$ [47] as a function of distance d according to the following equation,

$$P_{TRG}(d) = \frac{P_t G_t G_r h_t^2 h_r^2}{d^4 L} \tag{4.3}$$

where, P_t ,G_t and G_r were defined before, h_t and h_r are the heights of the transmitting and the receiving antenna respectively. Here, the path loss factor L is assumed to be equal to unity by default. The operating frequency band is set to $915MHz$ and the raw over the air data rate corresponding to this frequency band is set to 40kbits per second. The routing protocol, packet size, and the traffic type are set as indicated in Table 4.1. The simulation was executed by placing the routers at 200m, 300m, 350m, and 450m apart. In this experiment, the source (Node 0) and the destination (Node 3) were always placed more than one hop distance apart as shown in Figure 4.4. This experiment is intended to evaluate the effects of packet losses in the network based on the distance between router nodes and based on node failure scenarios. The node failure cases were simulated in three separate scenarios by causing a node close to the gateway to fail and a node far from the gateway to fail. One more test case was also considered where one node close to the gateway and another node far from the gateway fail simultaneously. This particular experiment was set

up such that Node 0 (coordinator) sends data to Node 3 (end device) while the other Nodes act as routers. A constant bit rate traffic was set up between Node 0 and Node 3. Random sized packets with a maximum allowed size of 128 bytes were sent continuously at a time interval of 100 milliseconds between the packets and the simulation was run for a period of 20 seconds. Upon successful completion of the simulation, NS-2 simulator outputs a trace file which contains the information about the number of packets generated, number of packets dropped, number of packets received, number of packets sent and number of packets lost in the network. The output trace file is then read into another tool called as tracegraph, which helps in parsing the trace file and outputs the packet statistics as shown in Figure 4.8. The packet loss percentage is calculated by using,

$$Packet\ Loss\ Percentage = (\frac{Number\ of\ Packets\ Lost\ \mathbf{x}\ AveragePacket\ Size}{Number\ of\ Bytes\ Sent})\ \mathbf{x100} \tag{4.4}$$

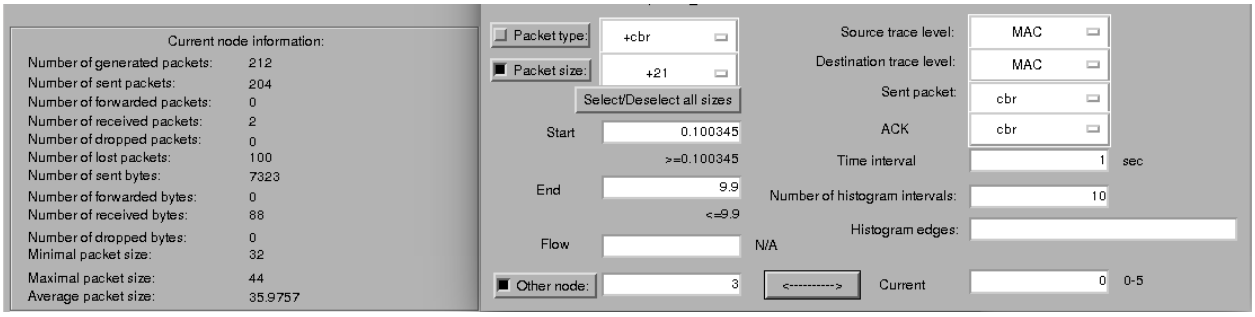

Figure 4.8: Tracegraph Output Window.

In this experiment, the node failure cases were introduced by simply moving the nodes out of the transmission range of all the other nodes. The node failure cases also were analyzed by keeping the nodes apart at different distances away from each other. It is interesting to note that the location of node failure also has an impact on the percentage of packets lost. Figure 4.9 shows how the percentage of packet losses scale as a function of the distance between the nodes when all nodes are healthy and also when there are node failures. It can be noted that, when all nodes were healthy, packet losses don't occur until 300m and there is

some packet loss observed when the nodes are placed at 350m apart. This is consistent with the earlier test that was conducted to estimate the range of XBee's in an environment that was obstacle prone. As the distance between the adjacent nodes is increased, the percentage of packet loss also increased. Another interesting fact that can be noted from Figure 4.9 is that the percentage of packet losses are higher when a node close to the gateway fails as opposed to the failure of a node far from the gateway. This is because, when node 2 fails, during the process of flooding, Nodes 5 and 4 will try to flood the packets to Node 1, causing the communication channel of Node 1 to be always busy. This results in more number of re-transmissions and reception timeouts which ultimately translates to lost packets. The situation becomes even worse when two routers fail in the network shown in Figure 4.9. This happens because there is only one path from source to destination and in a ground level sensor network scenario, it is highly probable that this path is obstacle prone which decreases the effective transmission range.

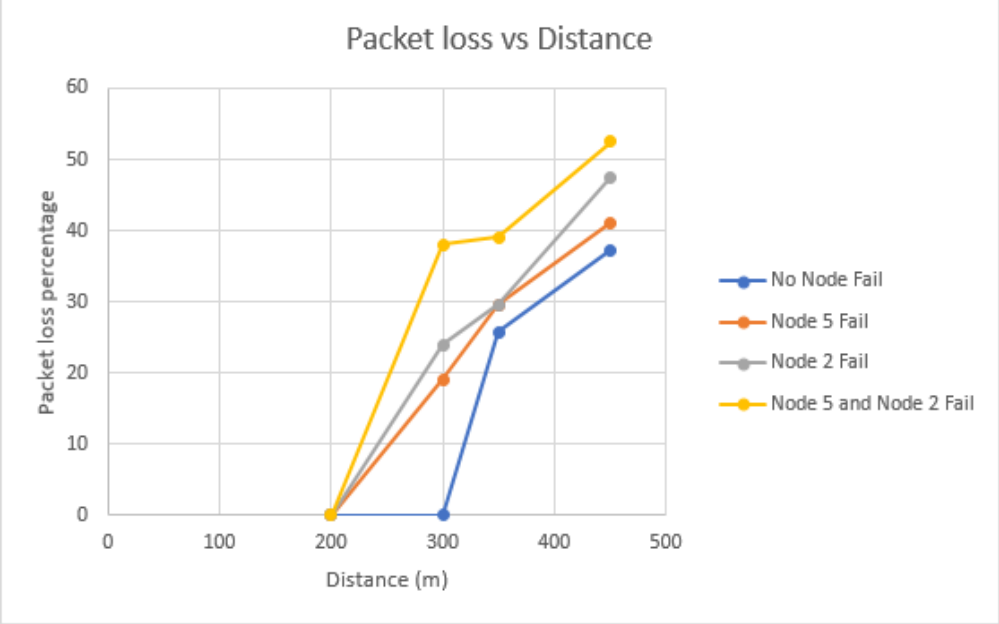

Figure 4.9: Packet Loss Percentage as a Function of Distance.

4.4 GSM Communication

GSM functionality is exclusive only to the gateway in the EMS network. The GSM module that is currently being employed is the UBLOX SARA-U260, which is a 3G module with 2G fallback compatibility. SARA-U260 supports High-Speed Packet Access (HSPA)/GSM bands in North America [49]. High-Speed Packet Access (HSPA) is compliant with 3G technology while the Global System for Mobile Communication (GSM) is compliant with the 2G operating technology. SARA-U260 module can be coupled with T-Mobile and AT&T sim cards in North America. The radio communication features supported by AT&T are HSPA, High-Speed Uplink Packet Access (HSUPA) and High-Speed Downlink Packet Access (HSDPA), in 3G operating mode, while also supporting LTE. T-Mobile, on the other hand, supports GSM and Enhanced Data Rate for GSM Evolution (EDGE), both of them being 2G operating modes. T-Mobile also has support for HSPA, HSUPA, HSDPA, and Long Term Evolution (LTE). In addition, T-Mobile supports General Packet Radio Service (GPRS) mode of communication, in which the network providers charge only for the amount of data used and not for the duration of data used in this mode. GPRS is a packet-based data service system that establishes communication with web applications through TCP/IP sockets which can then be used to make HTTP (Hyper Text Transmission Protocol) POST requests to the server. Additionally, HSPA and other LTE modes on the SARA U-260 modules are not optimized for power consumption. GPRS mode consumes less than a third of the amount of power that is consumed in HSPA mode [49]. Since EMS only sends 128 bytes of data per transaction, it is unnecessary to operate the SARA-u260 module in the high-speed HSPA or LTE modes. Hence, GPRS has been chosen as the preferred mode of communication.

The SARA U-260 module is interfaced with the ARTIX-7 FPGA through a UART bus, configured in the interrupt mode. Configuration and data transfer with the SARA-U260 module is done with the help of AT commands. Firstly, it is necessary to configure the module with the appropriate Access Point Name (APN) , which is specific to the network

provider. The APN must be written into the nonvolatile memory of the SARA-U260 device, before using it to send data to the park station. A GSM data transmission outlining the following process is shown in Figure 4.10. Once data packets are received from the slave module, the XBee interrupt lines are disabled and the GSM interrupt lines are enabled. This is done to ensure that the GSM UARTS have full control over the MicroBlaze interrupt lines until the data is transmitted. The configuration written in the non-volatile memory of the GSM device is first read by the application layer of the GSM module. The GSM module is then configured to communicate in GPRS mode. Next, a valid port number is assigned to be able to send POST requests through TCP/IP sockets. The port number is set to 80 because the HTTP internet communication protocol uses Port 80 by default. HTTP POST requests containing source counts, GPS coordinates, and sensor data are then sent to the server application script that is written in PHP. As the server application receives the ASCII data from the EMS board, data is parsed into variables. Single alphabetic letters are used as parsing delimiters to reduce the amount of data sent per report. The variables are then processed to convert them into appropriate units (SI) and stored in a MySQL (Structured Query Language) database. The SQL database can then be queried to read each field and plot the metrics on the website.

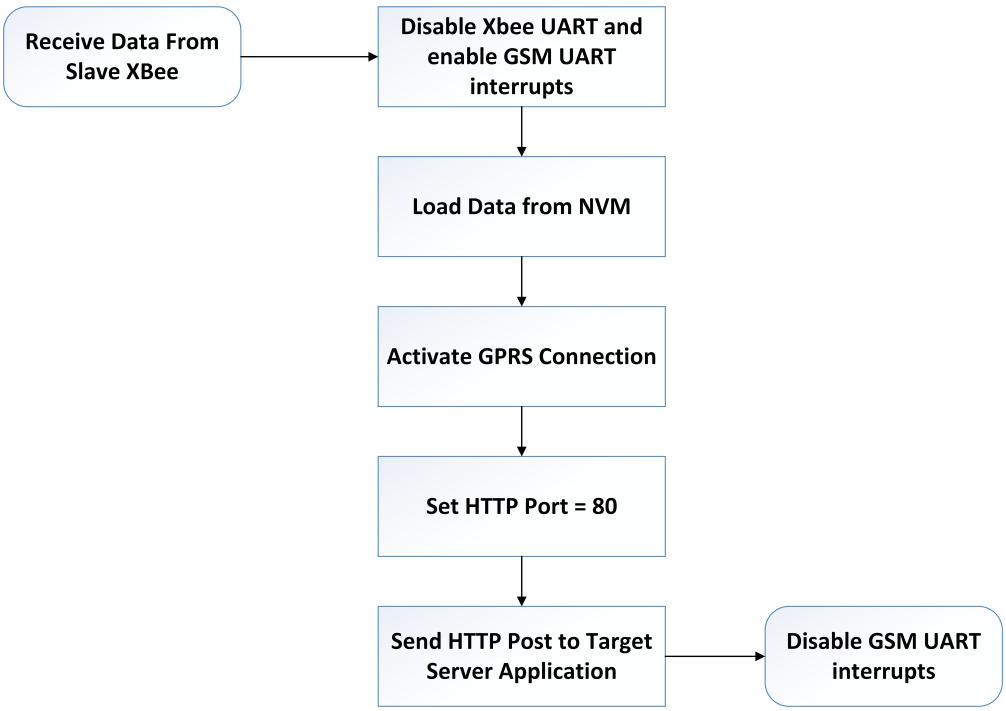

Figure 4.10: GSM Configuration Flowchart.

While preparing the report, the slave module associates each of the sensor values, GPS coordinates, source counts with single alphabet variable names to keep the payload size as small as possible. The string needs to be compatible with the HTTP query format, for example,

"A=1&B=185719200618&C=3558.6804&D=N&E=11450.2284&F=W&G=555&H=3260"

where the variable 'A' is the field name, '1' is the field value and so on. It is necessary to use the ampersand symbol as a field differentiator. While preparing the string, the variable names used in the MicroBlaze firmware must be exactly the same as the ones used in the PHP script, so that the raw data sent from the EMS board can be parsed and plotted on the website accurately.

Updating Detection Threshold Values through GSM: As mentioned previously, the EMS system makes decisions using two detectors. The transient event detector looks for the presence of sources under the assumption that none were previously present while the quiescent detector looks for the spectral features that correspond to the end of the dominant source event. The detection threshold values of these detectors need to be experimentally determined and set before deploying the EMS system in the field. Currently, in the EMS system, there is a provision to update these values from a remote location by sending text messages to the GSM module as described in Figure 4.11.

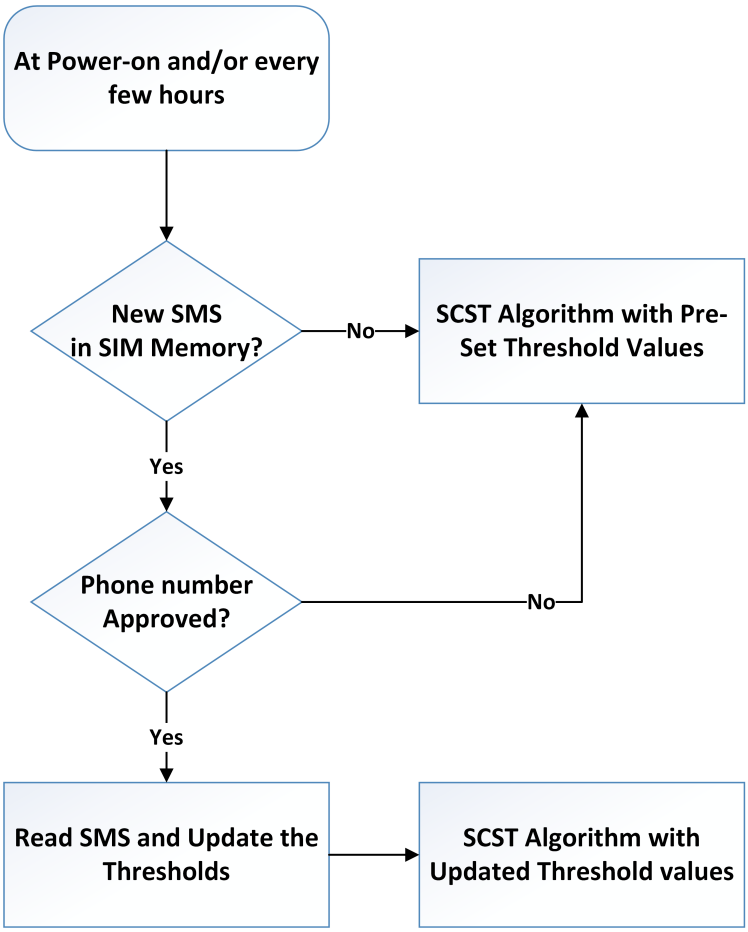

Figure 4.11: Updating Detection Thresholds via SMS.

The GSM module is configured to accept text messages only from phone numbers that are present in the approved list and text messages from other sources are deleted. The text messages are configured to be stored in the SIM card memory to keep track of the received

messages in an orderly manner. As can be seen from Figure 4.11, the thresholds can be updated either at power-on and/or once every few hours (whenever the EMS sends reports to the web server). The approved user has to send the text message in the prescribed format for example: "S100" or "s100" and "N010" or "n010" for updating transient and quiescent detection thresholds, respectively. It must be noted that if the text messages are not in the prescribed format, they will be discarded. The format, however, can be changed in the future to suit the requirements.

4.5 Conclusion

The EMS system is designed to collect acoustic data, perform near real-time processing on the data and send out periodic reports about the classified sources and the environmental parameters. Every EMS node is equipped with a low power XBee transceiver, which allows multiple EMS systems to be easily deployed in the form of an intelligent network in national parks. As mentioned in this chapter, the XBee uses a process is known as route discovery to dynamically estimate a routing path. That is, the EMS network can be designed to be self-forming and self- healing, especially when there is more than one path from the source to destination. This also indicates that new nodes can be easily added or the existing nodes can be removed from the EMS sensor network without disturbing the functionalities of other nodes. Ground reflections play a major role in reducing the transmission range of the XBee. This issue can be minimized by mounting the XBee antennae on a high post to avoid these reflections. An experiment was conducted to study the variation of the packet loss percentage with respect to the location of the node failure. It was observed that more packets are lost when a router node close to the gateway fails as opposed to the case where a router far from the gateway fails. However, it is to be noted that, the environment where the data was collected for the XBee range test consisted of interference from steel and various ground automobiles such as cars, buses, etc. These sources of interference are unlikely to be present deep within national parks. This would mean that, potentially, a better transmission range

can be expected from the XBee modules, provided the antennae are kept sufficiently off the ground. EMS gateway is equipped with the GSM facility which is used to send data to a park station. It has to be noted that the gateway must have good cellular connectivity at all times to ensure the reports are reliably sent to the park station as there is currently no efficient way to build redundancy into the system to deal with this issue. But as addressed in Section 4.4, it is known that SARA-U260 module supports T-Mobile and AT&T carriers, and these two network providers combined, provide sufficient coverage throughout out the US. Hence, EMS, as it is, should be deployable in most national parks.

CHAPTER 5

FIELD TEST RESULTS

5.1 Introduction

Two EMS systems were recently deployed at the Lake Mead National Recreation Area, where one system (slave) was deployed for the purposes of detection and classification, while the other EMS system served as the master or gateway to the park station. The slave module performed the detection and classification while also collecting the information about the surrounding environment such as air pressure, temperature, etc and sent these reports to the gateway wirelessly through the XBee link. The main function of the gateway was to collect the data sent by the slave node through the XBee module and then hand over those reports to the park station with the help of the onboard GSM module. The slave module was first trained based upon annotated and labeled 1/3 octave data previously collected over a 48-hour period (from 7/5/2016 to 7/7/2016) at Lake Mead National Recreation Area (different physical location). The training involved building the dictionary matrices using the K-SVD algorithm [18] for different source types and interference present at that particular site and computing the log-likelihood values for each Bayesian network source model. These dictionary matrices and log-likelihood values were then stored in the flash memory of the EMS slave node. The system was specifically trained to detect and classify helicopters and jets as these were the dominant sources of interest present at this particular site.

This chapter mainly focuses on analyzing the system performance and deployment limitations using the results obtained during the recent field test conducted in Lake Mead National Recreation Area. Section 5.2 focuses on explaining the experimental setup used in the field test. Section 5.3 focuses on the analysis of the results and concluding remarks are presented in Section 5.4.

5.2 Field Test Set Up

The trained system along with the gateway were deployed during June 20 to 21, 2018 in Temple Bar Marina, located in the Lake Mead Recreational Area. The deployment location was not the same as the one that was used to collect the training data. As a result, it was important to re-evaluate the detection and quiescent threshold values before deploying the systems to conduct a full system test.

As mentioned before, the detection and classification tasks on the EMS is done in two phases: 1) signal detection to locate the presence of a transient signal of an unknown source under the assumption that none were present and 2) quiescent detection to find the end point of the transient signal by searching for observations where the particularly dominant source is no longer present under the assumption that there was one present. Hence, the EMS system was set up for a test run for an hour or so in the field to obtain the $1/3rd$ octave data and also the log-likelihood ratios computed by the SCST algorithm, in the presence of helicopter sources. The collected data was then plotted using MATLAB to visually correlate the detection results corresponding to the generated $1/3rd$ octave spectral images in order to set the right threshold values before the system was actually deployed. These tests were conducted multiple times by re-configuring the EMS board each time with quiescent threshold values namely, 5, 30, 50 while keeping the transient detection threshold value at 100. The test conducted by keeping the quiescent detection threshold at $\gamma = \mathbf{1}0$ and the transient detection threshold at $\eta = \mathbf{1}00$, yielded acceptable results for the helicopter class. The high energy signatures shown by the yellow markings in the $1/3rd$ octave spectral image in Figure 5.1a indicates the presence of helicopter sources. The quiescent and transient threshold values are also displayed in Figures 5.1b and 5.1c. When the quiescent statistic of a particular source type crosses the pre-set threshold ($\gamma = \mathbf{1}0$), end of the source is declared and the winning source is classified. As can be seen from Figures 5.1a, 5.1b and 5.1c, the detection results correlate well visually with the $1/3rd$ octave data. Hence the EMS was reconfigured with these quiescent and transient detection threshold values for this test.

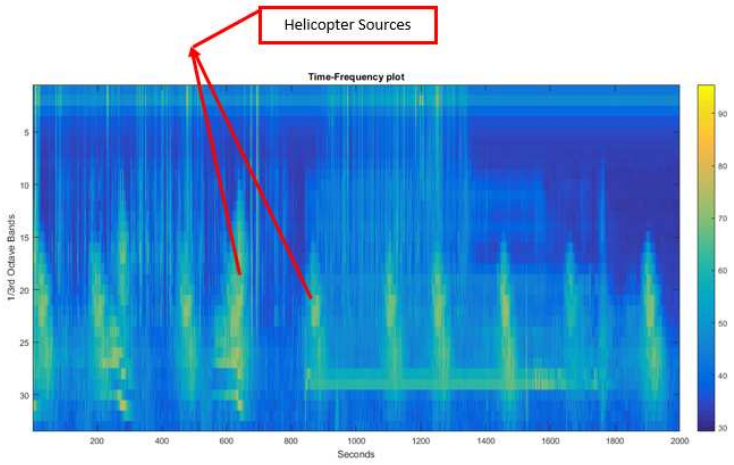

(a) $1/3rd$ Octave Plot.

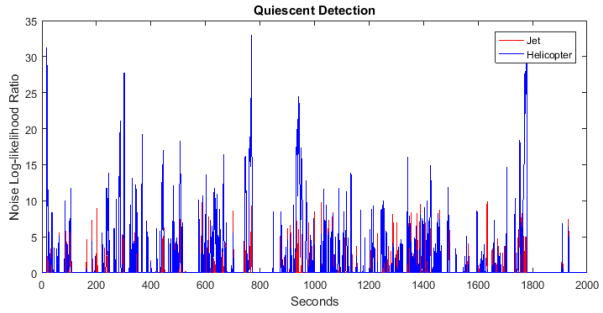

(b) Noise Log-likelihood ratio.

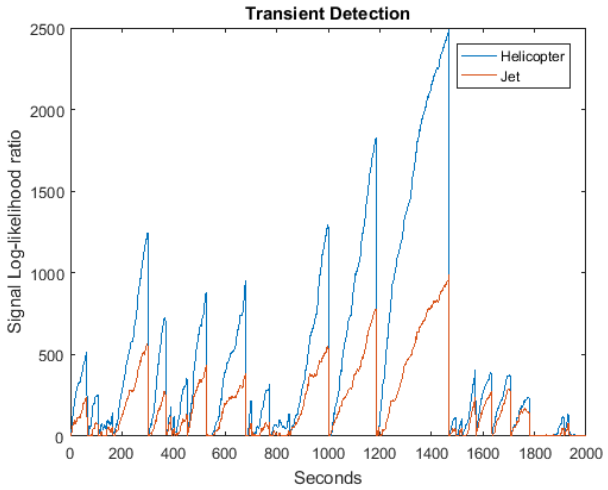

(c) Signal Log-likelihood ratio.

Figure 5.1: Detection and Classification Results.

To keep the EMS systems secure during the field test they were put in modified pelican cases to ensure where the antennae are not enclosed within the case as shown in Figures 5.2b

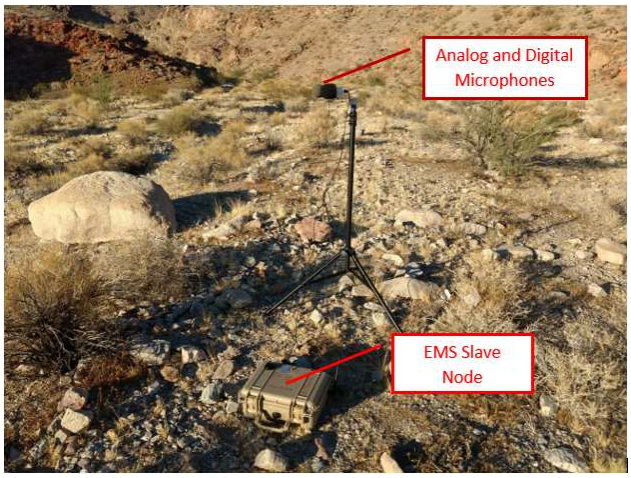

(a) EMS slave node with microphone.

(b) Pelican Case architecture for Slave node.

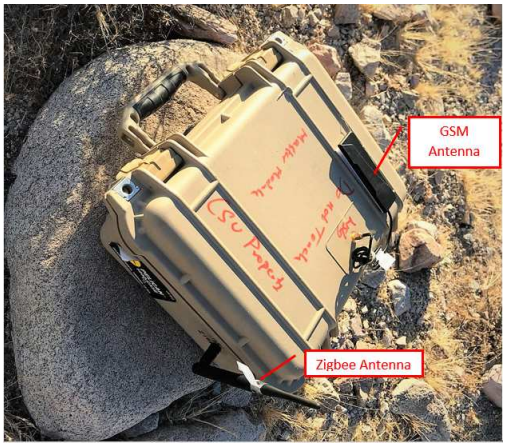

(c) Pelican Case architecture for Master node.

Figure 5.2: EMS Field Deployment.

and 5.2c. The antennae of GSM and the GPS modules were connected to the case by using suitable male-female SubMiniature Version A (SMA) extension cables and adapters, while the XBee antenna was connected using reverse polarity SMA cables. The slave module was connected to the digital microphone (Ivensense ICS-43432) and the time-series of the events were recorded by using an audio recorder whose input lines were connected to an analog microphone as shown in Figure 5.2a. The deployment set up for slave node along with the microphones are shown in Figure 5.2a.

The test was conducted in a location which was exposed to a good amount of source

traffic and had adequate cellular connectivity. After configuring the EMS board with the new detection threshold values, the slave and master modules were deployed by placing them approximately 300 meters apart. The EMS boards were programmed to send reports once every 3 hours to the park station and these reports were used to plot the source classification details and also the environmental data on the website. The GPS coordinates of the slave node are sent to the gateway and are used to pinpoint the exact location of the EMS node which is displayed on the website with the help of google maps as shown in Figure 5.3. During this field test, the gateway node was not equipped with a GPS module.

Lat	Long	NodeID	Helicount AVG	Jetcount AVG
36.026	-114.682	1	22.967	0.067

Figure 5.3: GPS coordinates and Average Source count data.

The helicopter and jet counts were reported by the EMS system for every three hours time interval as well as on a daily basis for over a period of thirty days. These plots are displayed on the website as shown in Figure 5.4 and can be used to extract useful information about the traffic distribution of the sources throughout the day and also over the entire month.

As mentioned previously, the EMS also reports the information about the surrounding environment to the park station. These reports contain information related to air pressure, PCB temperature, availability of sunlight in the area and the exact orientation of the system.

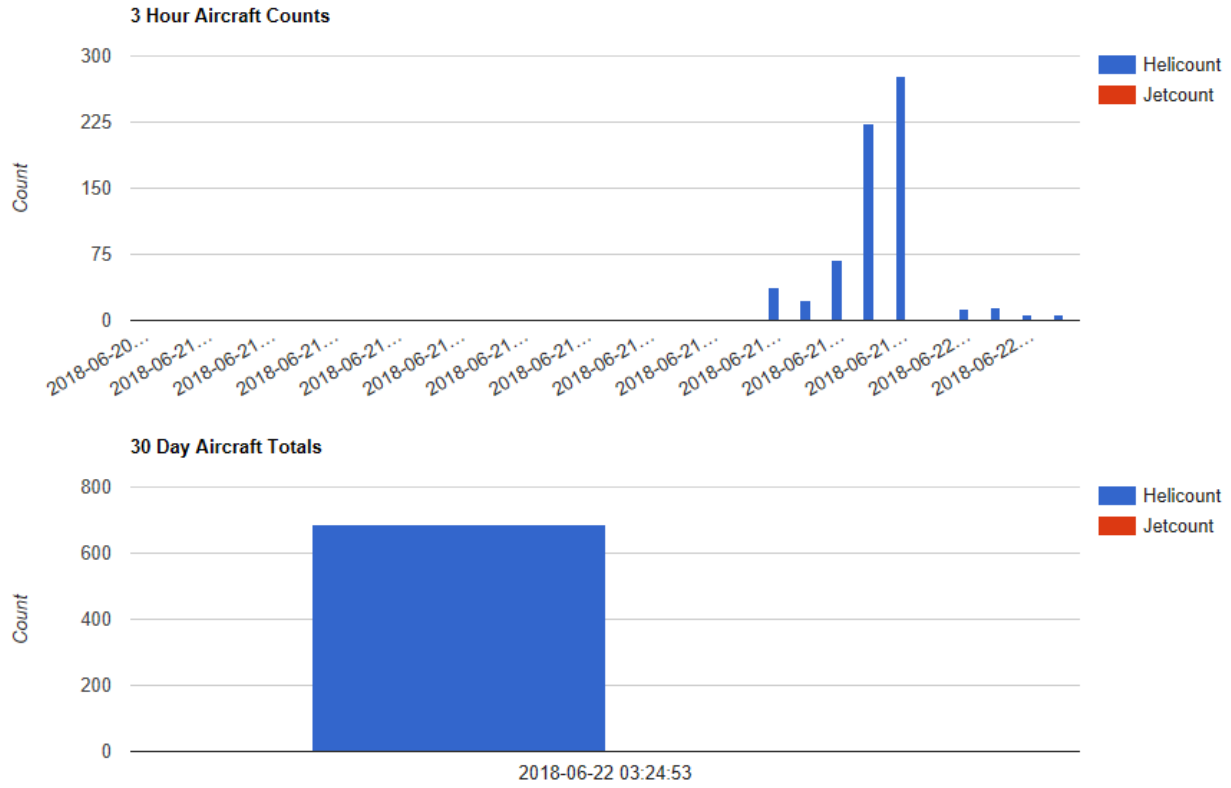

Figure 5.4: Aircraft Counts Reported on the EMS Website.

The sensor data collected during the field test are also provided on the EMS website. For the period of our tests, these plots that were generated and shown in Figures 5.5 - 5.9 correspond to 3-axis digital accelerometer, PCB temperature, air pressure, light sensor, and 3-axis digital compass, respectively.

It is important that the onboard electronic components always operate well within the specified operating temperature range. During the field test, it was noticed that the PCB temperature measured by the onboard sensor reached as high as 65 degree Celsius. It is possible that the temperatures could get close to the operating temperature limit of some of the onboard electronic components. It should also be noted that the Li-ion battery that was used in this field test has an optimal temperature range from 0° - 45° Celsius. The battery life and the charge acceptance will significantly reduce as the operating temperatures increase beyond the optimal range [50]. The PCB temperature plots serve as an important tool to monitor these factors and take appropriate actions to fix them. The light sensor data

shown in Figure 5.8 can be used for power management purposes by powering down some non-essential systems when there is not much sunlight available to operate the system and charge the battery. The 3-Axis digital compass data shown in Figure 5.9 can be used to assess the precise orientation of the microphone array and the system in the beamforming algorithm to estimate accurate Angle of Arrival (AoA) of the sources. This information was not used in this study.

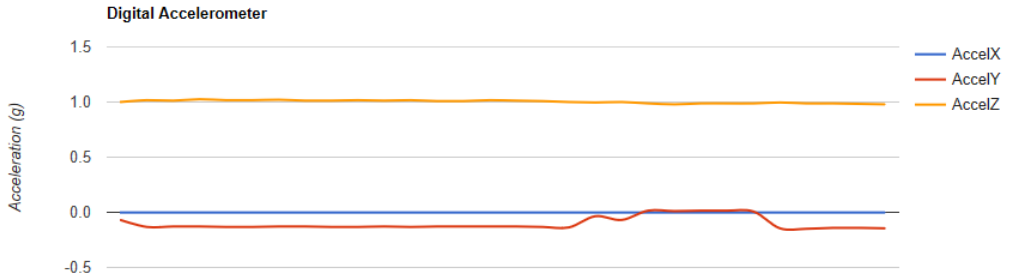

Figure 5.5: 3 Axis Digital Accelerometer Data.

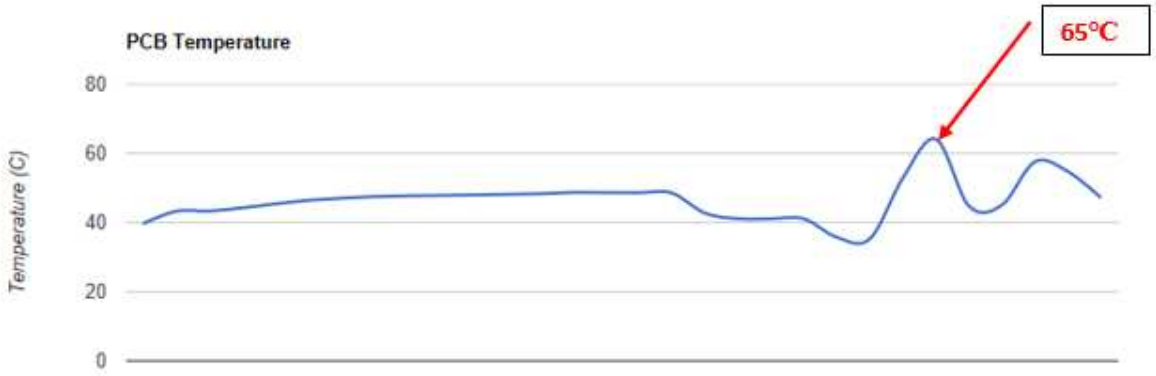

Figure 5.6: PCB Temperature.

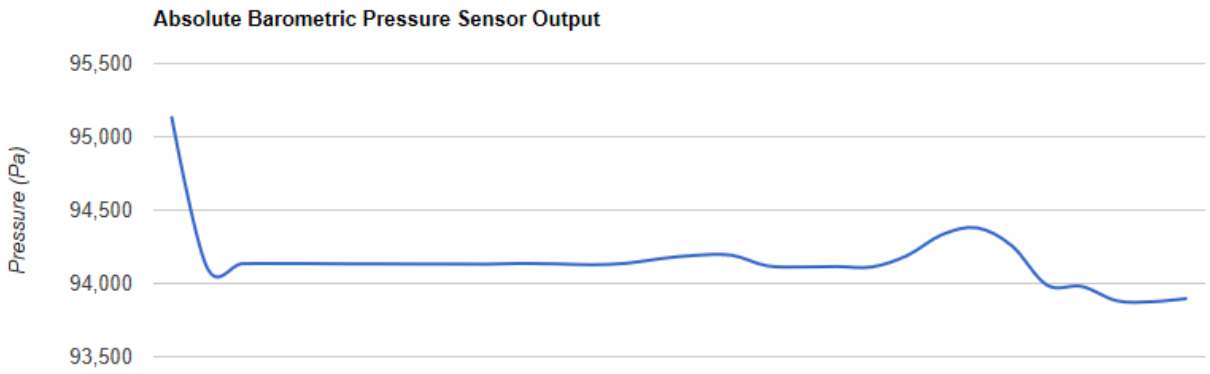

Figure 5.7: Absolute Barometric Air Pressure.

Figure 5.8: Light Sensor Data.

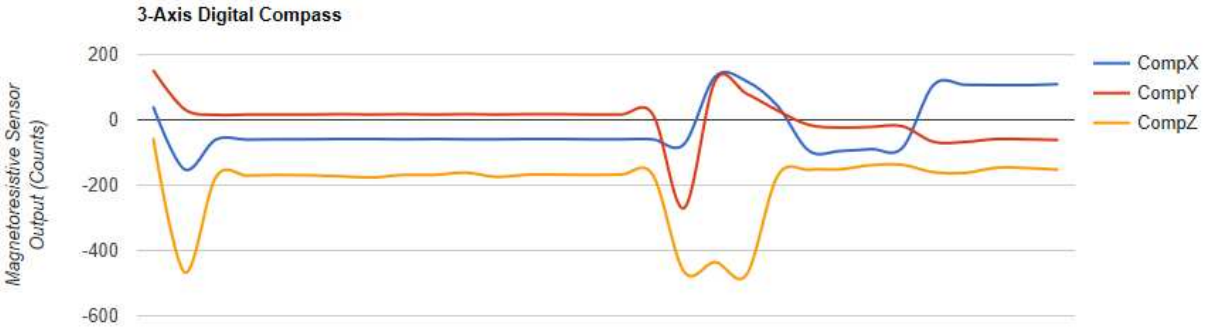

Figure 5.9: 3-Axis Digital Compass

5.3 Field Test Results and Observations

As shown in Section 5.2, the EMS system was able to perform detection and classification of the sources, collect environmental data, and report all of this information automatically to the park station. The detection and classification results in Figure 5.4 indicated that the

EMS system reported more than 600 helicopters while identifying only a few jet sources. These results might suggest that there could have been quite a bit of misclassification of the jet class. The helicopter sources occur more frequently compared to the jets because of high traffic due to air tours at this particular park. Since the helicopters fly at a much lower altitude compared to the jets, their acoustic signatures are also stronger (i.e, higher SNR). There was also a significant amount of propeller plane traffic in the area and their acoustic signature resembled very closely with those of the helicopter sources and could have led the EMS system to misclassify them as helicopters. This is mainly due to the fact that the training data for the system did not include any examples of the propeller plane sources [8]. Additionally, the training data was collected in a windy environment and labeling of this data was performed by visual evaluation of the $1/3rd$ octave spectrum and also by listening to the actual time-series data recorded during the system deployment. From the audio data, it was evident that the acoustic signatures produced by the jet sources closely resembled strong wind hence, causing misclassification and false alarms. Insufficient training data (imbalance) pertaining to the jet class also indicates that the system was not trained well to identify all cases of jet sources. Another key factor for classification error can be attributed to the fact that the system was not deployed in the same location that was used to collect the training data. This indicates that the SCST algorithm is not robust enough to a substantial variation of location and needs to be trained on a larger set of data containing both helicopter and jet sources to perform accurate detection and classification irrespective of where it is deployed as the surrounding landscape has a huge impact on the captured acoustic signatures.

From the communication system standpoint, it was observed that the Lake Mead National Recreational area does not have good cellular coverage in general, especially deeper within the park. Even though there are a few cell phone towers present around the Lake Mead area, the range of these towers is limited by terrain shielding caused due to the presence of hills and mountains. It was observed during the field test that the cellular service in this area is not reliable as the EMS system abruptly lost cellular connectivity for nearly nine hours and

had to be moved to a slightly different location before the tests were resumed again. Hence, it is important to thoroughly investigate the location and make sure it has good cellular coverage before deploying the system.

A range test similar to the one described in Section 4.3 was performed in the field before deploying the EMS systems. It was found that 300 meters separation between the slave node and the master node was approximately the farthest distance that the slave and master systems could be placed apart so that the no packets are lost at the time of XBee communication. At the time of this test, there was no provision to place the XBee antennae higher above the ground and the terrain shielding in the vicinity made it harder to achieve a higher transmission range for the XBee. The XBee PRO S3B module that was used during this test has a line of sight range up to 9 miles [34], provided there is absolutely no RF interference in the deployment region. Although it might not be possible to achieve this theoretical limit in the field, the transmission range of the XBee modules can be improved by placing them higher above the ground to avoid ground reflections as much as possible.

5.4 Conclusion

This chapter presented the results of our recent field test that was conducted in the Lake Mead National Recreation Area. Two EMS systems were deployed in the field, where one system was trained to perform detection and classification while the other system functioned as a gateway. The detection threshold values were determined in the field by conducting a test runs and visually evaluating the detection results collected during this test. Due to insufficient training data available for the jet source class, it was noted that the system wrongly classified a number of the jets as helicopters. The low detection threshold values may have caused the system to perform classifications even before there was enough confidence to make a decision. The detection and classification accuracy can be improved by re-training the EMS system with a larger set of data and by more accurately determining the detection threshold values by conducting multiple test runs in the field and verifying the onset and

endpoint of the detected sources as well as comparing the obtained classification results with a truth table.

The EMS systems were, however, able to autonomously perform detection and classification and send reports to a web server with the help of GSM and XBee modules. It was noted in Section 5.3 that, the GSM module lost cellular connectivity abruptly during the test. This was mainly due to the effects of terrain shielding in the deployment area. This issue can be overcome by thoroughly investing the deployment area and making sure that there is sufficient cellular connectivity before deploying the devices. It is also possible to add another gateway in the network as a means of redundancy to account for this failure. The transmission range of the XBee modules can be increased by placing the XBee antennae within the line-of-sight and by keeping the antennae sufficiently off the ground to minimize RF signal reflections.

CHAPTER 6

CONCLUSIONS AND SUGGESTIONS FOR FUTURE WORK

6.1 Conclusions

The work in this thesis focused on the development of the communication systems and their complete integration with the SCST algorithm and with the analog sensor suite on the ARTIX-7 FPGA-based EMS system. A $1/3rd$ octave filter bank is implemented on the FPGA to generate onboard near real-time spectral features of the captured acoustic signal. The SCST algorithm implemented on the MicroBlaze softcore processor uses the output of the $1/3rd$ octave filter bank to perform detection and classification tasks. The SCST algorithm currently implemented on the EMS was specifically trained to detect and classify the jet and helicopter sources. The classification results (source labels), along with the $1/3rd$ octave data is stored in the SD card, while the source counts are tracked using a counter. A fixed interval timer was implemented on the FPGA to time the reporting of the source events.

The EMS node that performs detection and classification, transmits the results along with the measured sensor data to a network gateway with the help of a XBee transceiver, once every few hours. The EMS node that is equipped with the GSM module acts as a network gateway and is responsible for posting the reports received from the other nodes onto a web server. A full system test was conducted by deploying two EMS nodes in the Lake Mead National Recreation Area during June 20-21, 2018. The EMS system was previously trained for detection and classification on the data captured over 48 hours during July 5-7, 2016 in Lake Mead Area, though deployed in a different location at much higher elevation.

The detection thresholds were experimentally determined and adjusted in the field to accommodate for this change in ambient noise levels and signal strengths. It was found that the EMS system frequently misclassified jets and propeller planes as helicopters. This is mainly due to a lack of robust training data. Moreover, the training data did not contain examples belonging to propeller plane class. Additionally, the acoustic signature of jets resembles that of strong wind which makes the decision-making challenging especially when the training dataset does not have enough samples of jets. It is also necessary to fine-tune some of the parameters including the detection thresholds and the dictionary matrices to improve the detection and classification performance of the algorithm.

As far as the communication systems are concerned, the XBee module was fully functional and the slave system was able to send classification reports (source counters) along with the measured sensor data to the master node (gateway) successfully. From the XBee standpoint, it was noted that the farthest the two EMS modules could be placed apart was approximately 300m to make sure that the packets were transmitted reliably at all times. This limitation was mainly because the XBee antenna was placed close to the ground which increased the likelihood of RF signal ground reflections, thereby reducing the effective transmission range. Moreover, there was an intermittent problem related to cellular connectivity in the deployment area. This issue can be addressed by thoroughly investigating the area and making sure that there is good cellular coverage before deploying the EMS systems.

6.2 Future Work

Although EMS systems demonstrated autonomous detection, classification and reporting of the source events, there is still some room for future work that needs to be done before the EMS systems can be deployed as an acoustic wireless sensor network in the field.

Robust Training : It was observed, during the field test, that the SCST algorithm performed many misclassifications. This is mainly due to lack of robust training data, particularly for jet and propeller sources. The EMS systems need to be trained more thoroughly by using a larger and more representative training data set for all source types present in the particular site. It is desirable to collect the $1/3rd$ octave training data from various parts of the national park to enable the SCST algorithm to accurately perform detection and classification independent of the deployment location. The detection threshold values also need to be fine-tuned to make sure that interference signals do not get detected as sources.

Expert Evaluation: It is highly recommended that the detection and classification results generated by the EMS be ground truth-ed by an expert from NPS to more accurately assess the source of mis-detections and misclassifications. This evaluation can also help in coming up with the right threshold values before the system is deployed in the field. It is possible that most of the acoustic data captured in the field is affected by the terrain itself and this factor needs to be accounted for while calculating energy values for the frequency sub-bands. It would be valuable to work with experts at NPS to come with the right models that can be incorporated in the firmware to cancel out this interference.

Network of Multiple Nodes : As mentioned before, we currently have only two fully developed EMS systems and hence we were able to achieve automatic report generation from a single node. This functionality needs to be expanded to multiple nodes to form a mesh network of EMS systems. This work requires configuring the XBees in the API mode and also changing the transmitting packet structure to API format as shown in Figure 4.2. The MicroBlaze firmware for the gateway also needs to be changed by adding an array of buffers to store the reports that are received from slave nodes to accommodate this feature. An array of buffers should be added to store the reports that are received from the slave nodes and data parsing code should be added to the gateway firmware as the received data will be in API format, unlike the raw format in AT mode.

Enclosure Design : As mentioned in Chapter 5, the high ambient temperature in the Lake Mead could pose a threat to the reliability of the onboard electronics. Hence, it is highly desirable to conduct an industrial grade environment test on the EMS boards to pre-assess their limitations during actual deployment. The EMS was enclosed within a pelican case as shown in Figure 5.2 and this rules out the usage of the light sensor to assess the ambient sunlight. This can make it challenging to asses when to use a battery and when to use solar mode during deployment. Hence, there is a need to come up with a new architecture for EMS casing to make sure that we are able to fully utilize the potential of the board while keeping it safe from the heat.

XBee System : An effort needs to be made to increase the transmission range of the XBees during deployment. This can be particularly hard to achieve as a line of sight for the XBee antenna cannot be guaranteed in the field. A solution is to couple the XBee with a high gain antenna to increase the RF signal transmit power. Moreover, the XBee antenna needs to be placed higher above the ground to minimize RF signal ground reflections and maximize the transmission range. The EMS can send reports to the web server only when there is cellular connectivity, and currently, there is no easy way to work around this problem. While it is possible to switch to a different wireless technology like LoRa (Long Range) LpWAN (Low-power Wide Area Network) by Semtech, instead of XBee, which is more suitable for wide area outdoor sensor networking, it is not recommended as it would require significant hardware and firmware changes. The best option we currently have is to increase the transmission range of the XBee by using a high gain antenna and to make sure the gateway is always present in a location where it is guaranteed to have good cellular connectivity. Since the main idea is to cover a larger area of the national park for noise monitoring, an option to alleviate this problem is, adding redundancy through the deployment of more number of slave nodes in the network to route the information to the gateway.

GSM System : Since the cellular connectivity in the deployment is often patchy, it is recommended to have more than one gateway in the network to account for losses. However, to accommodate this feature, extra firmware needs to be added in the slave module in-order to add the capability of routing the reports to another gateway when one fails. Another option is by storing the reports sent by the slave nodes in a file in First In First Out (FIFO) format at the gateway when cellular signal is not available. AT commands can be used to query the GSM module to assess the available cellular signal strength and as soon as the module returns acceptable values, the entire FIFO can be sent to the web server, one row at a time. With this approach, one can be certain to have an accurate alignment of the reports with the occurrences of the sources. This is because, each report string contains its own time-stamp and when the data is sent to the web server, the reports are automatically rearranged and displayed on the website in chronological order, irrespective of when they are sent.

BIBLIOGRAPHY

[1] J. G. Colonna, B. Gatto, E. M. D. Santos, and E. F. Nakamura, "A framework for chainsaw detection using one-class kernel and wireless acoustic sensor networks into the amazon rainforest," in *Proc of 17th IEEE International Conference on Mobile Data Management (MDM)*, vol. 2, pp. 34-36, June 2016.

[2] M. Hawkes and A. Nehorai, "Acoustic vector-sensor correlations in ambient noise," *IEEE Journal of Oceanic Engineering*, vol. 26, no. 3, pp. 337–347, Jul 2001.

[3] C. Salazar-Garca, R. Castro-Gonzlez, and A. Chacn-Rodrguez, "RISC-V based sound classifier intended for acoustic surveillance in protected natural environments," in *Proc of IEEE 8th Latin American Symposium on Circuits Systems (LASCAS)*, Feb 2017.

[4] A. Digulescu, M. Paun, C. Vasile, T. Petrut, D. Deacu, C. Ioana, and R. Tamas, "Electrical arc surveillance and localization system based on advanced signal processing techniques," in *Proc of IEEE International Energy Conference (ENERGYCON)*, May 2014.

[5] C. J. Baby, N. Munshi, A. Malik, K. Dogra, and R. Rajesh, "Home automation using web application and speech recognition," in *Proc of International conference on Microelectronic Devices, Circuits and Systems (ICMDCS)*, Aug 2017.

[6] M. A. Quintana-Surez, D. Snchez-Rodrguez, I. Alonso-Gonzlez, and J. B. Alonso-Hernndez, "A low cost wireless acoustic sensor for ambient assisted living systems," *Applied Sciences*, vol. 7, no. 9, 2017.

[7] *Model 831 Sound Level Meter Technical Reference Manual*, Larson Davis, 2006.

[8] V. Yaremenko, M. R. Azimi-Sadjadi, and J. Zacher, "Unattended acoustic sensor systems for source detection, classification, and tracking," *to appear, IEEE Transactions on Instrumentation and Measurement*.

[9] O. Postolache, P. Girao, and M. Pereira, "Underwater acoustic source localization based on passive sonar and intelligent processing," in *Proc of of IEEE Instrumentation & Measurement Technology Conference (IMTC)*, 2007.

[10] O. Postolache, M. D. Pereira, and P. Girao, "Intelligent distributed virtual system for underwater acoustic source localization and sounds classification," in *IEEE Workshop on Intelligent Data Acquisition and Advanced Computing Systems: Technology and Applications*, Sept 2007.

[11] F. Pianegiani, M. Hu, A. Boni, and D. Petri, "Energy-efficient signal classification in ad hoc wireless sensor networks," *IEEE Transactions on Instrumentation and Measurement*, vol. 57, no. 1, pp. 190–196, January 2008.

[12] S. Haykin, *Neural Networks and Learning Machines*. Prentice Hall, 2003.

[13] D. Moore, "Demonstration of bird species detection using an acoustic wireless sensor network," in *Proc of 33rd IEEE Conference on Local Computer Networks (LCN)*, Oct 2008.

[14] J. Sallai, W. Hedgecock, P. Volgyesi, A. Nadas, G. Balogh, and A. Ledeczi, "Weapon classification and shooter localization using distributed multichannel acoustic sensors," *J. of Systems Architecture: Embedded Systems Design*, vol. 57, no. 10, pp. 869–885, 2011.

[15] P. William and M. Hoffman, "Classification of military ground vehicles using time domain harmonics' amplitudes," *IEEE Transactions on Instrumentation and Measurement*, vol. 60, no. 11, pp. 3720–2731, November 2011.

[16] S. Akhtar, M. Elshafei-Ahmed, and M. Ahmed, "Detection of helicopters using neural nets," *IEEE Transactions on Instrumentation and Measurement*, vol. 50, no. 3, pp. 749–756, June 2001.

[17] N. Wachowski and M. Azimi-Sadjadi, "Detection and classification of nonstationary transient signals using sparse approximations and Bayesian networks," *Audio, Speech, and Language Processing, IEEE/ACM Transactions on*, vol. 22, no. 12, pp. 1750–1764, December 2014.

[18] M. Aharon, M. Elad, and A. Bruckstein, "K-SVD: An algorithm for designing overcomplete dictionaries for sparse representation," *IEEE Transactions on Signal Processing*, vol. 54, no. 11, pp. 4311–4322, 2006.

[19] F. V. Jensen, *Bayesian Networks and Decision Graphs*. Springer, 2001.

[20] A. Lozano and A. Carlosena, "DSP-based implementation of an ANSI S1.11 acoustic analyzer," *IEEE Trans. on Instrumentation and Measurements*, vol. 52, no. 4, pp. 1213–1219, August 2003.

[21] N. Wachowski, "Characterization of multiple time-varying transient sources from multivariate data sequences," Ph.D. dissertation, Colorado State University, 2007.

[22] M. Azimi-Sadjadi, A. Pezeshki, and N. Roseveare, "Wideband DOA estimation algorithms for multiple moving sources using unattended acoustic sensors," *IEEE Transactions on Aerospace and Electronic Systems*, vol. 44, no. 4, pp. 1585–1599, October 2008.

[23] *Ivensense ICS-43432 Data Sheet*, Ivensense Inc., 2016.

[24] A. Irturk, B. Benson, and R. Kastner, "An efficient FPGA implementation of scalable matrix inversion core using QR decomposition," *UCSD Technical Report, CS2009-0938*, 2009.

[25] *AXI Interrupt Controller (INTC) v4.1*, Xilinx, April 2018.

[26] M. R. Azimi-Sadjadi, J. Kopacz, and N. Klausner, "K-SVD dictionary learning using a fast OMP with applications," *Proc of IEEE International Conference on Image Processing (ICIP)*, October 2014.

[27] J. N. Tsitsiklis, "Extremal properties of likelihood-ratio quantizers," *IEEE Transactions on Communications*, vol. 41, no. 4, pp. 550–558, April 1993.

[28] "Specification for octave, half-octave, and third octave band filter sets," *ANSI S1.11-2004*, 2004.

[29] "Electroacoustics - octave-band and fractional-octave-band filters - part 1: Specifications," *IEC 61260-1:2014*, 2014.

[30] John.G.Proakis and D. G. Manolakis, *Digital Signal Processing Principles, Algorithms and Applications*. Prentice Hall International INC, 1996.

[31] U. Meyer-Baese, *Digital Signal Processing with Field Programmable Gate Arrays*. Springer.

[32] M. Martinez-Peiro, J. Valls, T. Sansaloni, A. P. Pascual, and E. I. Boemo, "A Comparison between Lattice, Cascade and direct form FIR filter structures by using a FPGA bit-serial Distributed Arithmetic Implementation," in *Proceedings of ICECS '99, The 6th IEEE International Conference on Electronics, Circuits and Systems*, 1999.

[33] *Elimination of Limit Cycles and Overflow Oscillations in Time-Varying Lattive and Ladder Digital Filters*, no. STAN-M-35, San Jose, CA, USA, 05/1986 1986. [Online]. Available: https://ccrma.stanford.edu/files/papers/stanm35.pdf

[34] *DIGI XBEE-PRO XSC - Data Sheet*, DIGI International, 2018.

[35] *IEEE Standard for Local and metropolitan area networks - Part 15.4: Low-Rate Wireless Personal Area Networks (LR-WPANs)*, IEEE, 2011.

[36] *Zigbee Alliance*, 2018, http://www.zigbee.org/.

[37] H. Sizun, *Radio Wave Propagation for Telecommunication Applications.* Springer, 2005.

[38] *900 MHz versus 2.4 GHz*, 2018, https://www.digi.com/resources/standards-and-technologies/rfmodems/frequency-comparison.

[39] "IEEE standard for low-rate wireless networks," *IEEE Std 802.15.4-2015 (Revision of IEEE Std 802.15.4-2011)*, April 2016.

[40] J. Hofhiens, *WF101: RF Essentials.* DIGI.

[41] A. Lozano and A. Carlosena, "Ad hoc on-demand distance vector routing," *Technical Report*, July 2003.

[42] M. Marti, *Directed Flood Routing Framework.* Institute for Software Integrated Systems, Vanderbilt University, Nashville, TN, USA, 2004.

[43] DIGI, *XBee-PRO 900HP/XSCRF Modules S3 and S3B*, 2018.

[44] T. Issariyakul and E. Hossain, *Introduction to Network Simulator 2 (NS2).* Springer US, 2012.

[45] M. Hilman, "An overview of zigbee networks," *MWR infosecurity.*

[46] DIGI, *XCTU Configuration and Test UtilitySoftware*, 2018.

[47] T. S. Rappaport, *Wireless communications, principles and practice.* Prentice Hall, 1996.

[48] H. L. Bartoni, *Radio propagation for Modern Wireless Systems.* Prentice Hall, 2000.

[49] UBLOX, *SARA-U2 series HSPA modules with 2G fallback.*

[50] *BU-410: Charging at High and Low Temperatures.*, 2018. [Online]. Available: http://batteryuniversity.com/learn/article/charging